Annals of Nuclear Energy 157 (2021) 108212

Contents lists available at ScienceDirect

Annals of Nuclear Energy

journal homepage: www.elsevier.com/locate/anucene

Studies of reactor noise response to vibrations of reactor internals and thermal-hydraulic fluctuations in PWRs

V. Verma [a,*], D. Chionis [b], A. Dokhane [a,*], H. Ferroukhi [a]

[a] Paul Scherrer Institute, Laboratory for Reactor Physics and Thermal-Hydraulics, CH-5232 Villigen PSI, Switzerland
[b] Axpo Power AG, Nuclear Energy Division, Parkstrasse 23, CH-5401 Baden, Switzerland

ARTICLE INFO

Article history:
Received 26 October 2020
Received in revised form 5 February 2021
Accepted 18 February 2021
Available online 6 March 2021

Keywords:
Neutron noise
Fuel assembly vibration
Thermal-hydraulic fluctuations
Core-barrel vibration
Time-domain
CASMO-5
SIMULATE-3K

ABSTRACT

This work is a contribution towards the development of computational methods that allow investigation and prediction of reactor noise response due to in-core perturbations such as vibrations of reactor internals and fluctuations in thermal-hydraulic parameters. Further improvements are made to the modelling approach to allow for vibrations of fuel assemblies at higher vibrational modes. Modelling of such realistic noise sources, and assessment of the induced noise response are presented in this paper. Results show that the simulation of individual noise sources and their combinations affect the neutron noise phenomenology. The neutron noise induced radially and, in particular, axially, reflects the imposed vibrational patterns associated to the higher modes of the fuel assemblies. The results provide confidence in the application of the developed methodology based on commercial time-domain codes for modelling of realistic noise scenarios and numerical noise analyses of the PWR cores.

1. Introduction

In a nuclear reactor system, several sources of perturbations are responsible for the fluctuations seen in the neutron density, even during normal steady-state conditions. These sources include the neutronic parameters, thermal-hydraulic parameters such as inlet coolant temperature, coolant flow blockage, and excessive vibrations of reactor core internals such as control rods, fuel assemblies and core barrel due to strong hydraulic and mechanical forces. The fluctuation that reflects the inherent stochastic nature of neutrons is known as neutron noise, where noise refers to the deviation of a time-dependent quantity, i.e. neutron flux, from its mean value. The neutron noise signal, as measured by the online detection system composed of in-core and ex-core neutron detectors, is a useful quantity for monitoring the status of the reactor and diagnosing for possible anomalies. The modelling of the perturbation sources and simulation of the induced neutron noise is performed as part of neutron noise analysis of a reactor core. It is a commonly used non-invasive reactor surveillance technique as it offers a complement to the protection and control systems and an alternative to the wide range of diagnostic instrumentation that is difficult to install given the space constraints in a reactor core (Pázsit et al., 2010). The neutron noise is broadly classified in two categories: zero-power noise and power-reactor noise. The former refers to the neutron fluctuations due to random phenomena at low power, where no external reactivity effects result from change in power and temperature. The latter, which is the scope of this paper, refers to the neutron fluctuations resulting from reactivity changes due to neutronic, thermal and mechanical perturbations in power reactors (Thie, 1981).

Over the last decade, some of the KWU pre-KONVOI PWRs in Spain, Germany and Switzerland encountered operational problems when the neutron noise levels increased systematically in the core over several reactor cycles (Almaraz Trillo Report, 2012). Some of these reactors were forced to operate at a reduced power as the abnormal increase in the neutron noise levels triggered the reactor protection system in such cases, thereby, affecting the availability of the plants. It was observed that the abnormal noise behavior coincided with the installation of a new fuel assembly type in the core whose design was suspected to be prone to lateral vibrations during operation (Seidl et al., 2015). Excessive vibrations of the structural components, in particular, fuel assemblies' vibrations, therefore, were identified as one of the plausible causes. The partially unexplained origin of the abnormal noise level increase is the motivation behind the CORTEX project (CORe monitoring Techniques and EXperimental validation and demonstration), which is funded by the European Commission, and aims at developing innovative core monitoring techniques that are capable of detecting,

* Corresponding authors.
E-mail addresses: vasudha.verma@psi.ch (V. Verma), abdelhamid.dokhane@psi.ch (A. Dokhane).

https://doi.org/10.1016/j.anucene.2021.108212
0306-4549/

identifying and localizing anomalies in power reactors (Demaziere et al., 2018). From an industrial perspective, in order to ensure continued and reliable reactor operation, it is necessary to determine the sensitivity of reactor parameters to the in-core perturbations.

Since the early 70s, neutron noise diagnostics have been used for surveillance activities in both PWRs and BWRs for monitoring the normal operation of nuclear reactors, the early detection of anomalous behavior, diagnosing the anomaly and consequently, predicting the outcome. Neutron noise methods are either based on studying the dynamic response of the reactor to the in-core perturbations, or based on analyzing the induced neutron noise obtained via in-core and ex-core detection systems (Thie, 1981).

Some of the reactor applications of neutron noise based methods, during power operations in BWRs, are channel-type boiling instabilities, steam velocity and void measurements. Other applications in different power reactors include core barrel vibrations, fuel motion and individual fuel rod/assembly vibrations, fuel failure, absorber vibrations i.e. control rod movements, and changes in temperature coefficient, among others (Pázsit et al., 2010). Few of these perturbations are covered in this paper, as described in later sections. Early efforts for noise diagnostics methodology included solving noise equations analytically for simple systems, and later numerical methods for calculating neutron noise in heterogeneous systems (Demazière, 2017; Pazsit et al., 1998; Sweeney et al., 1985; Bastl and Bauernfeind, 1975). With renewed interest in noise applications in the last decade and availability of vast computational resources, several research organizations are developing calculation tools to model and simulate neutron noise phenomena in the time- and/or frequency domain. In particular, CORE SIM is a MATLAB-based dedicated noise solver of the two-group neutron-noise diffusion equations in the frequency-domain, which has been verified against many semi-analytical reference solutions for several noise applications (Demazière, 2011; Demazière et al., 2015). Although CORE SIM has been validated for neutron noise simulations, such efforts have been limited to the analysis of coarse-grid configurations in the past. On-going development is now focused on more solvers that are accurate and can perform detailed simulations in a finer-grid (Mylonakis et al., 2020). The existing commercial time-domain based reactor-dynamics code such as SIMULATE-3K (S3K), although not primarily developed for noise applications, has been adapted to model fuel assembly vibrations and thermal hydraulic fluctuations (Chionis et al., 2020; Bermejo et al., 2017) with some limitations. Advancements have been made in the code and the methods to model realistic noise sources, as will be seen in this paper. Other commercial time-domain based codes, including DYN3D and PARCS have been adjusted for modelling noise sources such as absorber of variable strength and a travelling perturbation (Viebach et al., 2019; Olmo-Juan et al., 2019). DYN3D, along with a model based on fluid structure interactions, is being considered for modelling fuel assembly vibrations (Viebach et al., 2019). A new 2-D Method of characteristics based noise solver in APOLLO3, and a dedicated time-domain diffusion based noise solver FEMFFUSION is under-development for noise applications (Gammicchia et al., 2020; Vidal-Ferràndiz et al., 2020). In addition, another approach proposes Monte Carlo based algorithms to solve the neutron-noise transport equations in the frequency-domain (Yamamoto, 2018; Rouchon et al., 2017). These codes express in-core perturbations as either fluctuations of macroscopic cross sections, or in more physical terms, as time-dependent vibrations of fuel assemblies due to fluid-structure interactions.

At the Paul Scherrer Institute (PSI), the methodology under development for simulating numerical neutron noise in PWRs is based on the time-domain approach. The methodology consists of the in-house CMSYS platform based on the CASMO-5 (C5)/SIMULATE-3 (S3) code system, coupled with S3K, a multi-physics nodal core dynamics solver. The PSI neutron noise methodology is based on the, so-called, 'delta-gap model' in C5 and 'assembly vibration model' in S3K for modelling vibrations of fuel assemblies (Ferrer, 2015; Grandi, 2011). The delta-gap model in the lattice 2-D code C5 generates two-group macroscopic cross sections for water-gap variation representative of static fuel assembly displacement. This is complemented by the S3K based assembly vibration model, which imitates time-dependent lateral movements of fuel assemblies in x- and/or y-directions by dynamically modifying the water-gaps surrounding the oscillating fuel assemblies. This is in addition to the dynamic calculation capabilities of S3K for simulating thermal–hydraulic fluctuations. Recent studies systematically analyzed the capabilities of the CMSYS codes for modelling fuel assembly vibrations through a series of verification and qualification case studies at both lattice (C5) and nodal (S3K) level (Chionis et al., 2020). The impact of variation of water-gap widths on the cross sections produced via the C5 delta-gap model was successfully compared against the Monte-Carlo Serpent2 code (Leppänen et al., 2015). Further, the time-dependent variation in cross sections due to varying delta-gaps was incorporated in S3K to imitate fuel assembly vibrations of a single assembly and a cluster of assemblies, and the study of induced neutron noise phenomenology confirmed the validity of the model. These works have immensely contributed to the development of the PSI methodology to perform numerical neutron noise analyses for various perturbation scenarios in PWRs. While the above-mentioned studies have successfully demonstrated the qualification and robustness of the methods by verifying the induced neutron noise characteristics against measured plant data (Chionis et al., 2017), they have also highlighted several shortcomings. The studies were limited to the modelling of vibrations of one or more clamped-free fuel assemblies, unsupported from both ends, which are unrealistic movements in a reactor core. Typically, fuel assemblies are clamped to the core support plate, which modifies their vibrational behavior, as the fuel assemblies are no longer free to oscillate laterally on both ends. Such modelling limitations have prompted further developments in the neutron noise methodology by including dynamic axial vibrations to allow the modelling of higher vibrational modes of the fuel assemblies that are realistic in nature.

This paper presents the extended PSI neutron noise methodology that allows for realistic modelling of various perturbation scenarios present in PWRs such as movement of fuel assemblies at higher vibrational modes and core barrel vibrations, in combination with the thermal–hydraulic fluctuations of inlet coolant temperature and coolant flow. It qualitatively assesses the radial and axial neutron noise behavior in the core by evaluating the patterns of neutron noise amplitude and phase for certain perturbation parameters, and analyse the induced noise spectrum. The methodology is, therefore, capable of modelling and assessing the most plausible noise sources present in a PWR, and forms the basis of development of neutron noise monitoring system for nuclear reactors. Within the context of the CORTEX project, the current methodology was employed to generate simulated datasets for various different realistic scenarios based on the noise sources mentioned above, for the consortium partners. The simulated scenarios were representative of the real plant conditions as close as possible. The generation of simulated data containing nodal neutron fluxes and detector signals is essential for further performing advanced signal processing and training machine learning algorithms, as is shown in the recent works of the consortium partners (Durrant et al., 2019; Tasakos et al., 2021; Torres et al., 2019). The machine learning models are trained for anomaly characterization and localization purposes using the labeled simulation data, and later the techniques are applied on real plant. Eventually, such

techniques along with the simulation methods could be used for both online and offline core diagnostics and monitoring of the PWRs.

The paper is structured as follows. The description of the noise sources is given in Section 2. The detailed calculation methodology, including description of the core design, simulation tools and the modelling approach used to model fuel assembly vibrations using C5 and S3K, are given in Section 3. The simulation results illustrating neutron noise amplitude and phase induced by several noise sources in the core are discussed in Section 4 and Section 5, followed by the limitations of the neutron noise analysis model in Section 6 and conclusions in Section 7.

2. Sources of neutron noise

Even after careful design optimization that takes into account effects of irradiation, and thermal–hydraulic and mechanical forces such as flow-induced vibrations, yet, reactor internals' vibrations are observed within the PWR core. The spectral analysis of the neutron noise obtained from the KWU pre-KONVOI reactors reveals multiple peaks at specific frequencies that are representative of the noise sources in the core (Thie, 1981). The natural oscillations of the structural components of the reactor core, including the fuel assemblies, core barrel and reactor pressure vessel, are accompanied with random fluctuations of the thermal-hydraulic parameters, namely the inlet coolant temperature and coolant flow. Some of those noise sources that are modelled in this paper are described here.

As reported in (Thie, 1981), out of the various possible modes of fuel assembly vibrations, the most significant ones are the cantilevered mode at 0.6–2.0 Hz, where the fuel assembly is clamped-free at the top but fixed at the bottom; and the C-shaped and the S-shaped modes at 0.8–4.0 Hz and 5.0–10.0 Hz, respectively, where the fuel assembly is fixed at both the top and the bottom. The three vibrational modes are illustrated in Fig. 1. The mechanical properties of the fuel assembly, including the structural integrity and the length determine their frequency of vibration. The fuel assembly vibration resembles a damped spring with hysteresis, which is a close first-order mechanical description of such a perturbation. The typical displacement of the fuel assemblies is in submillimeter range.

Core barrel vibrations usually occur at overlapping frequencies with fuel assembly vibrations. The PWR core barrel is vertically suspended from the vessel top in a cantilevered fashion, leading to vibrations of the barrel at natural modes like beam mode and shell mode with respect to the reactor pressure vessel. The introduction of the coolant into the reactor pressure vessel through the cold legs at high velocities and subsequently, the large cross-flow of coolant in the PWR core results in a vibrating system through strong hydraulic forces. The two modes of vibration are illustrated in Fig. 2. The beam mode, which is the first mode of core barrel vibration, is in low submillimeter range (~60 μm) oscillating at a frequency of 8.0 Hz (Montalvo et al., 2016). The variation of gap between the core barrel and the vessel is slightly different at the core-top from the core-bottom as the barrel vibrates in a cantilevered manner in the beam mode. The so-called shell mode, which occurs at 20.0–25.0 Hz and resembles a changing circumferential shape, is not considered here as it occurs at frequencies much higher than the range of interest (Demazière and Dokhane, 2019).

Furthermore, the perturbations due to fluctuations in thermal–hydraulic parameters such as inlet coolant temperature and inlet coolant flow are significant at low frequency range of up to 2 Hz (Seidl et al., 2015). The coolant flow conditions affect the neutron moderation and consequently, the neutron noise spectrum in the core.

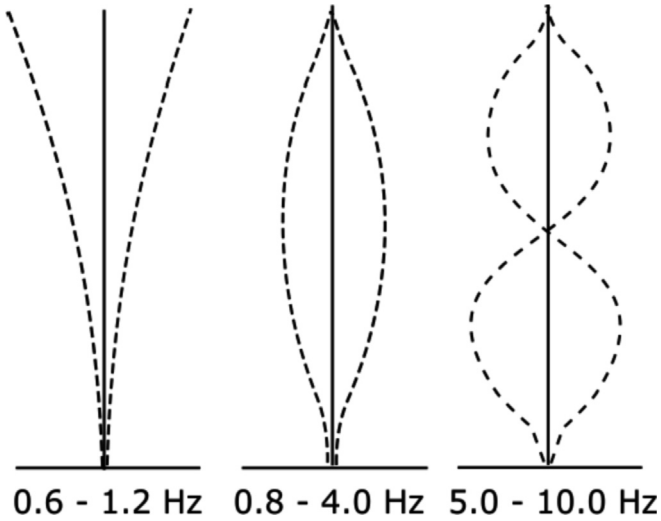

Fig. 1. Modes of fuel assembly vibrations – Cantilevered, C-shaped and S-shaped mode along with the frequency range of vibration.

3. Calculation methodology

The extended neutron noise methodology including the CMSYS codes used to model neutron noise sources at the lattice and nodal level, along with the simulation tools developed for reactor diagnostics and neutron noise analysis at PSI is described in this section. The in-core perturbations that are indeed the sources of neutron noise in the core are expressed in terms of variations in assembly-homogenized macroscopic cross sections.

A typical four-loop Westinghouse 15 × 15 mixed core PWR of the OECD/NEA transient benchmark is used for the study (Kozlowski and Downar, 2006). A radial layout of the core, along with an axially discretized single fuel assembly containing 32 nodes, are shown in Fig. 3. Eight radial in-core neutron detectors are modeled at six axial locations each, and four ex-core neutron detectors are modeled at two axial locations each.

3.1. Calculation approach and used codes

The three main steps involved in the modelling of fuel assembly vibrations, along with the simulation codes within the CMSYS code package are described here. In the first step, C5, a multi-group two-dimensional lattice code for modelling light water reactor fuel, where the transport solution is based upon the Method of Characteristics, is employed to generate two-group homogenized macroscopic cross sections accommodating for the varying water-gap widths using the 'delta-gap model'. This is in addition to the

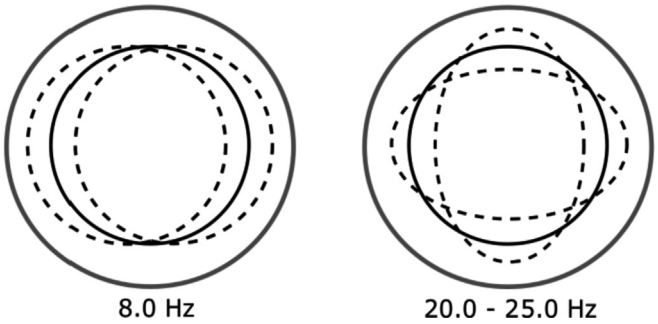

Fig. 2. Beam (left) and shell (right) modes of core barrel vibration. The core barrel (black) is vibrating w.r.t the pressure vessel (grey).

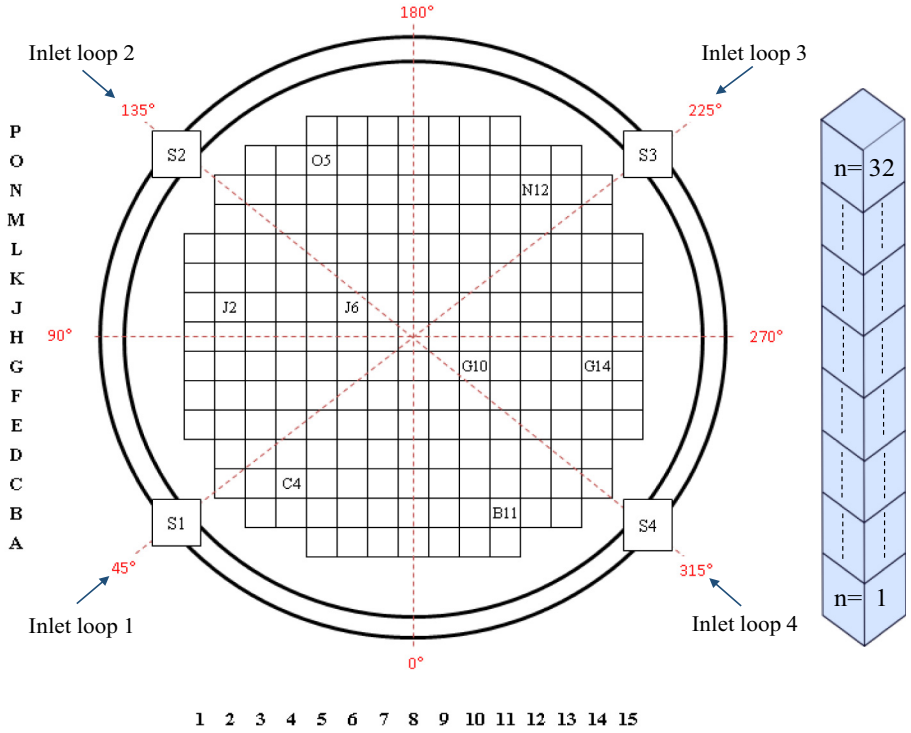

Fig. 3. Left: Radial layout of the OECD-PWR core model along with the labelled locations of the in-core, ex-core neutron detectors and the coolant loops. Right: Axial cross section of a fuel assembly with 32 nodes.

default automated branch case matrix capability for cross section generation that the code is used for, typically. It is assumed here that the lateral vibration of a fuel assembly can be represented as modification of the water-gaps surrounding the moving fuel assembly, instead of modelling physically oscillating fuel pins, and by extension, fuel assemblies. That is, when a fuel assembly moves δ mm in the positive x-direction, the surrounding water-gap increases by δ mm in the negative x-direction and decreases by δ mm in the direction of fuel assembly motion. A detailed study of the validity of this assumption is done in a previous work (Chionis et al., 2020). Initiating the delta-gap model, C5 performs an additional delta gap branch calculation, allowing the modification of the water-gap widths on the sides of the vibrating fuel assembly and generating corresponding perturbed macroscopic cross sections and discontinuity factors for the downstream codes S3 and S3K. In principle, the delta-gap model is capable of introducing water-gap widths on any of the four faces of the assembly, i.e. North, South, East and West. It is to note that C5 does not perform an added branch calculation for the generation of cross sections corresponding to negative delta-gap widths for PWR fuel assemblies. The cross sections corresponding to the negative delta-gap widths are obtained in the latter steps at nodal level by means of extrapolation.

CMS-LINK5 post-processes the C5 nuclear data that includes multi-group cross sections, discontinuity factors and kinetics data into a readable binary-formatted library for the downstream codes S3 and S3K for nodal full core calculations.

In the second step, three-dimensional nodal static core follow calculation is performed using S3, which is a multi-group nodal code for coupled neutronics and thermal-hydraulics analysis of LWR cores. It performs steady-state core-follow calculations to estimate nodal power and thermal–hydraulic state variables in the reactor core. Every fuel assembly is equally discretized into Z axial nodes, and every node is further split into 2×2 planar sub-nodes. The cross sections from C5 are homogenized within each such sub-node. S3 solves the three-dimensional two-group diffusion equation for every node for the static flux, and stores the state points in 'restart files' for the transient code S3K, corresponding to the operating conditions of interest.

In the last step, the three-dimensional two-group transient nodal code S3K is used to replicate time-dependent movements of the fuel assemblies through the 'assembly vibration model'. S3K allows simulating time-dependent vibrations of fuel assemblies in x- or/and y-direction by dynamically modifying the water-gap widths between any two fuel assemblies. To this aim, an in-house MATLAB script is used to create a support file for S3K containing water-gap widths between the fuel assemblies chosen for vibration and their adjacent assemblies, for each time step. The script allows the user to provide time-varying water-gap widths corresponding to different vibrational patterns in terms of choice of vibrating assemblies, and vibrational characteristics such as amplitude, phase and frequency, etc., and their combinations. In this modelling scheme, the vibration of a central fuel assembly affecting the water-gaps between the two neighboring fuel assemblies involves eight sub-nodes. A schematic diagram of the 'assembly vibration model' in S3K to illustrate the modelling of vibration of central assembly, FA_i, to the left direction is shown in Fig. 4. The vibration of fuel assembly is represented by introducing pre-calculated C5 cross sections corresponding to the modified water-gap width of $\delta/2$ in these eight affected sub-nodes, as marked in the Fig. 4.

Perturbed cross sections, $XS_{+\delta/2}$, corresponding to an increased water-gap width of $\delta/2$ are introduced in the four sub-nodes on the right, two each belonging to the oscillating assembly FA_i and the first neighbor, FA_{i+1}. Likewise, perturbed cross sections, $XS_{-\delta/2}$, corresponding to a decreased water-gap width of $\delta/2$ are introduced in the four sub-nodes on the left belonging to FA_i and FA_{i-1}. The fixed computational mesh in the core is conserved here. As mentioned earlier, the perturbed cross sections corresponding to the negative delta-gap widths that are missing in the pre-calculated

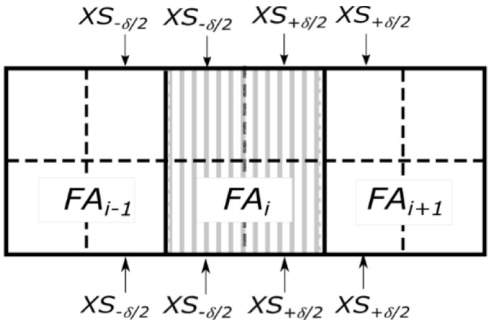

Fig. 4. Modification of cross sections when central FA, FA_i (striped) moves to the left direction. The modified cross sections, $XS_{-\delta/2}$ and $XS_{+\delta/2}$ are introduced in the eight labeled sub-nodes.

C5 nuclear data are obtained with S3K by extrapolating the values to delta gap width of – δ. Note that the maximum displacement amplitude of the fuel assemblies are limited by the distance between the neighboring fuel assemblies.

So far, the S3K version allows to model time-dependent simplistic vibrations of fuel assemblies only, where all the axial nodes in the vibrating fuel assembly are displaced by a constant and similar delta gap width. In this work, an enhanced version of the S3K is included in the modelling scheme for simulating more realistic time-dependent fuel assemblies' vibrations. The improved version with an updated 'assembly vibration model' contains a module that enables the user to impose pre-defined functions representative of the vibration modes of the fuel assemblies by assigning factored coefficients between zero and one to each axial node. In other words, the fuel assembly is modeled to vibrate in a certain axial pattern by displacing each of the axial nodes by a width, δ, that is calculated using the coefficients and the water-gap widths at every time-step. With the external support file generated with the in-house MATLAB script that contains time-wise delta-gaps, S3K performs transient full core calculations for a given set of operating conditions defined in the restart file from the previous step to calculate three-dimensional time-dependent two-group fluxes. This modelling scheme enables S3K to replicate time-dependent realistic movements of the fuel assemblies, and faithfully calculate the associated neutron noise source in the core.

In a reactor core, it is more likely that more than one fuel assembly is vibrating at the same time. The current model enables simultaneous displacement of multiple fuel assemblies in both synchronized and unsynchronized manner, at higher vibrational modes in two different directions with varying vibrational characteristics, i.e. amplitude and frequency, and patterns, i.e. random or sinusoidal, realizing modelling of realistic perturbation sources as close as possible. Core-barrel vibration is assumed to be seen as a collective movement of all the fuel assemblies in the core, and therefore, modelled based on similar principle as fuel assembly vibration. S3K contains an additional module that allows modelling of random fluctuations of thermal–hydraulic parameters, i.e. the inlet coolant flow, inlet coolant temperature and boron concentration, in all the four loops of the reactor in a synchronous manner. For inlet coolant temperature perturbations, non-synchronous fluctuations are also possible. The model includes a weight map for each coolant loop that defines the initial thermal–hydraulic parameters of the fuel assemblies belonging to that loop.

The fast and thermal neutron noise amplitude and phase is estimated from the nodal three-dimensional time-dependent neutron fluxes obtained with S3K. The radial and axial neutron noise distribution and its spectral characteristics such as coherence and power spectral densities (CPSD and APSD), obtained via standard signal processing techniques, are the quantities of interest in the neutron noise analysis. The signal processing technique involves a standard time- to frequency-domain analysis, which is based on the Fourier transform of the autocorrelation function. The extraction of signature frequencies is an effective way of identifying vibrational patterns in the core.

3.2. Calculation parameters

The perturbed cross sections are obtained via the implementation of the delta-gap model in quarter assembly symmetry in the lattice code C5. The lattice calculation approach is detailed in (Chionis et al., 2020). All the transient scenarios simulated with S3K are performed for a duration of 35 s at a time step of 0.01 s. A description of the basic scenarios is given in Table 1. The scenarios involving fuel assemblies' vibrations are modelled as synchronized pure sinusoidal vibrations along the x-direction with a maximum displacement amplitude of 0.1 cm, which is the typical half-distance between adjacent fuel assemblies in a KWU pre-KONVOI PWRs. It is to note that several other possible noise scenarios such as synchronized and unsynchronized random vibrations or noisy sinusoidal vibrations of fuel assemblies have been excluded from the analysis for the sake of brevity.

The PWR core comprises of 15 × 15 fuel assemblies and axially discretized into 32 nodes. The variation of the neutron fluxes in the fast and thermal groups, obtained with S3K at every nodal point in the core, is used to derive the induced neutron noise in terms of the statistical quantity, the coefficient of variation (CV). CV, expressed as percentage, is defined as the ratio of standard deviation σ to the mean value $\overline{\varphi}$ of the neutron flux φ in the energy group G, obtained at any given node located at i, j, z in the core. It is expressed as,

$$CV_G = 100 \cdot \frac{\sigma_{\varphi_G^{i,j,z}}}{\overline{\varphi}_G^{i,j,z}} \tag{1}$$

4. Neutron noise analysis of the transient scenarios

The results of the neutron noise analysis of the above-mentioned transient scenarios using S3K are presented in this section. The noise sources are introduced individually and in combination with each other. The analysis is focused on the verification of the modelling scheme, in particular the 'assembly vibration model' for modelling realistic vibrations of fuel assemblies and core barrel, and evaluating the qualitative and possibly quantitative impact on the induced neutron noise in the two energy groups for individual and combined scenarios.

4.1. Vibration of fuel assemblies at higher modes

Typically, fuel assembly vibrations have been found to occur in clusters in the core of LWRs, where the induced noise is dependent on several factors including the type of fuel assemblies, location, and fuel properties such as burnup, etc. Therefore, a systematic study of the vibration of a single fuel assembly and a group of assemblies, vibrating with different parameters is performed. The radial and axial distributions of the induced neutron noise due to the vibration of the central fuel assembly and the 5 × 5 central cluster are reported in this section. The radial and axial profiles of the fast and thermal neutron noise resulting from the vibration of a central fuel assembly (H8, as seen in Fig. 3) in the first vibrational mode, i.e. the cantilevered mode, are shown in Fig. 5. The pre-defined axial function representative of the vibrational mode is reflected in the induced noise profiles. The cantilevered beam mode, which is free at the top and attached to the core-support plate at the bottom, introduces larger water-gap width around the vibrating assembly at the top compared to the bottom, and

Table 1
Conditions of the basic simulated transient scenarios.

Transient scenarios				Vibrational frequency	Maximum radial displacement
1.	Fuel assembly vibration	a.	Cantilevered mode	1.2 Hz	1.0 mm
		b.	C-shaped mode	1.2 Hz	1.0 mm
		c.	S-shaped mode	5.0 Hz	1.0 mm
2.	Core barrel vibration	a.	Beam mode	8.0 Hz	60.0 μm
				Initial condition	Perturbation
3.	Coolant inlet temperature fluctuations			286.67 °C	±1 °C
4.	Coolant flow fluctuations			100%	±1%

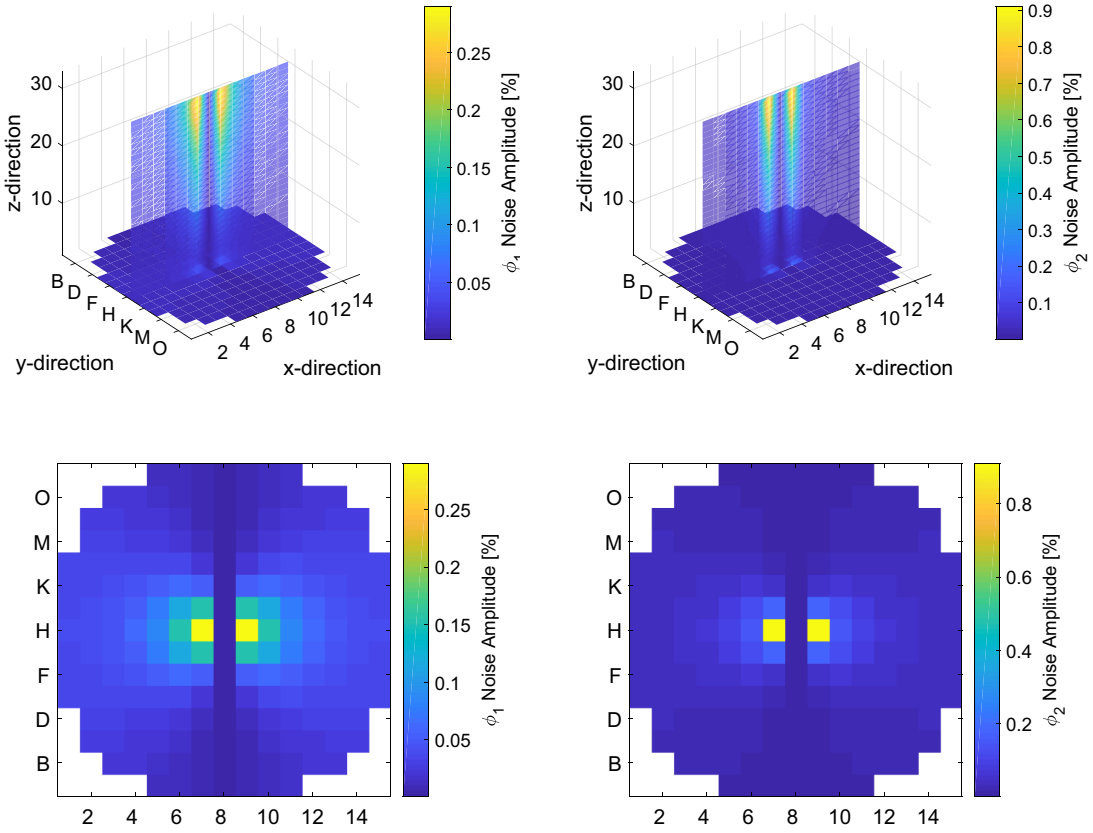

Fig. 5. Axial (top) and radial (bottom) distributions of the fast (left) and thermal (right) induced neutron noise due to vibration of the central fuel assembly (H8) in x-direction in the cantilevered mode at 1.2 Hz. The radial distributions are obtained at the axial node, Z = 31, where noise level is the highest.

therefore, higher neutron noise amplitude is obtained at the top of the assembly, as expected. For instance, the fast noise level at the top of the neighboring assembly is 0.30% compared to 0.01% at the bottom for a centrally vibrating fuel assembly. Similarly, the thermal noise level at the top is 0.90% compared to 0.06% at the bottom for a centrally vibrating fuel assembly. This is in contrast to the simplistic vibration mode modeled in previous works, where all the axial nodes were displaced with the same amplitude, and therefore, the axial induced neutron noise profile was almost axially uniform (Chionis et al., 2020). It is also seen that the induced noise at the center of the source is almost zero, while the maximum noise amplitude is obtained in the adjacent fuel assemblies along the direction of motion; the latter affected the most from the water-gap modification. This behavior is discussed in detail at the end of this section.

The fast and thermal neutron noise radial and axial profiles resulting from the vibration of a central fuel assembly (H8, as seen in Fig. 3) in the second and third vibrational mode, i.e. the C-shaped and S-shaped modes are shown in Fig. 6 and Fig. 7, respectively. The neutron noise profiles clearly follow the imposed noise sources, as expected, in the central fuel assembly modelled with the 'assembly vibration model' of the S3K. In case of the C-shaped mode, the core-lower and -upper support plates offer some resistance to the movement of assemblies from the bottom and the top, and introduces wider water-gap widths in the middle, which is reflected in the induced noise. The thermal noise level is 0.80% in the middle compared to 0.05% at the top and the bottom of the centrally vibrating assembly. The fast noise level is 0.25% in the middle compared to 0.01% at the top and the bottom of the centrally vibrating assembly. In case of the S-shaped mode, the time-dependent vibration of the fuel assembly is reflected in the noise distribution, as it appears to be split into two symmetric halves axially, representative of the S-shaped noise source. The highest thermal noise level is 0.79% and the highest fast noise level is 0.25%. The noise is higher at the top-half compared to the bottom-half due to the more negative moderator temperature coefficient of reactivity at the top, as explained later in this section. For all the scenarios of fuel assembly vibrations, the neutron noise distribution is symmetric around the oscillating fuel assemblies.

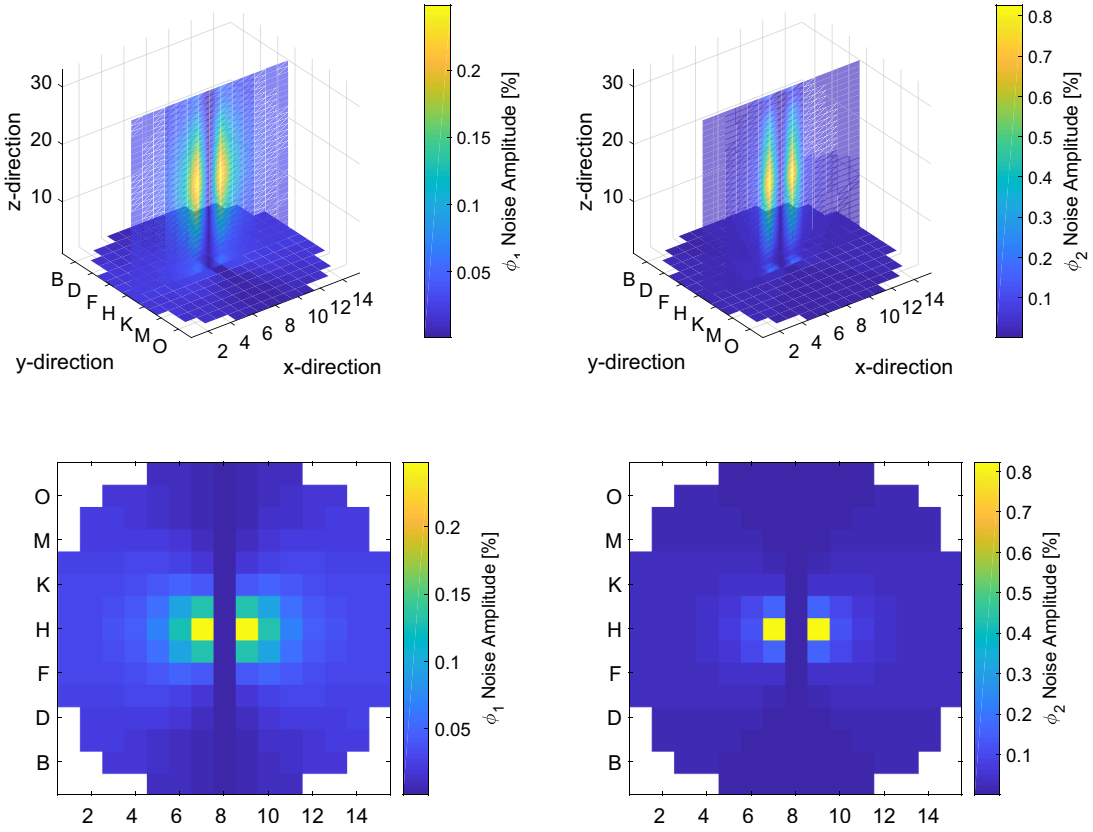

Fig. 6. Axial (top) and radial (bottom) distributions of the fast (left) and thermal (right) induced neutron noise due to vibration of the central fuel assembly (H8) in x-direction in the C-shaped mode at 1.2 Hz. The radial distributions are obtained at the axial node, Z = 16, where noise level is the highest.

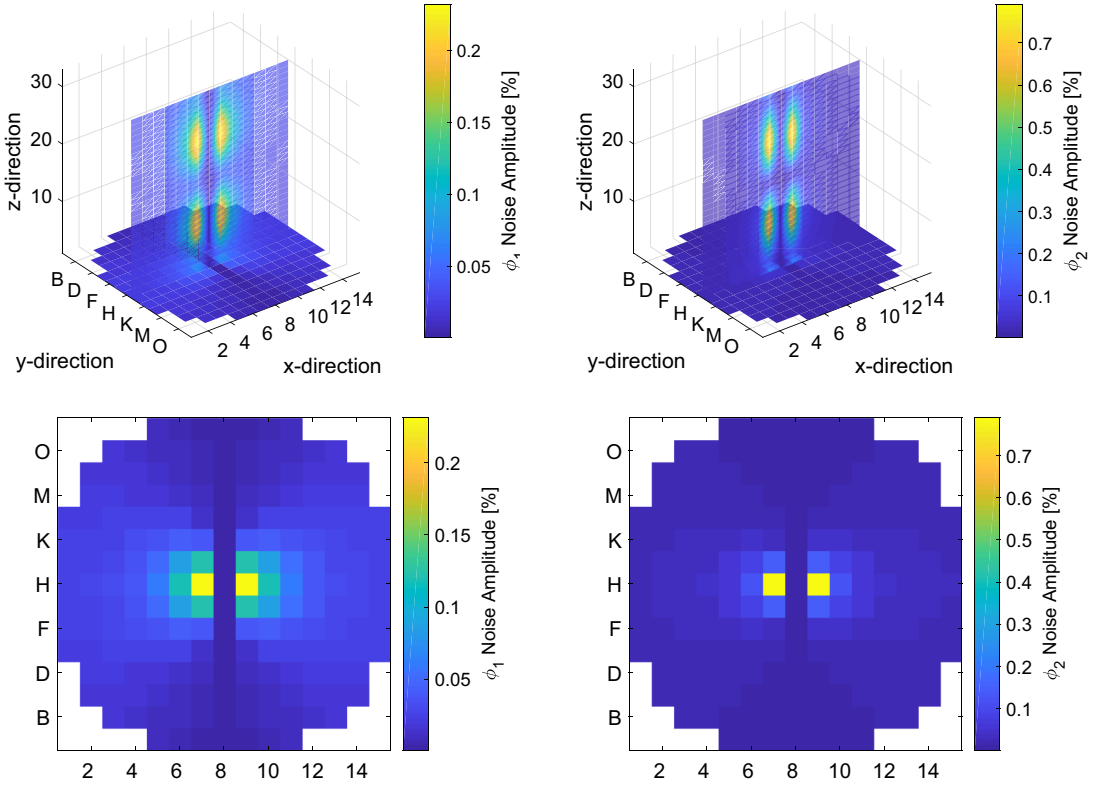

Fig. 7. Axial (top) and radial (bottom) distributions of the fast (left) and thermal (right) induced neutron noise due to vibration of the central fuel assembly (H8) in x-direction in the S-shaped mode at 5.0 Hz. The radial distributions are obtained at the axial node, Z = 24, where noise level is the highest.

It should be noted that the induced neutron noise amplitude is higher in the thermal group compared to the fast group due to the relatively larger capture and fission cross sections in the thermal energy region because of the water-gap increase. The fast neutron flux appears more diffused in the core owing to the larger mean free paths of fast neutrons compared to thermal neutrons. Overall, the neutron noise behavior is qualitatively consistent across both the energy groups in case of the three vibrational modes. However, as the dynamic variation of water-gap widths due to time-dependent vibrations of fuel assemblies affect thermal neutron noise the most, therefore, only thermal neutron noise profiles are shared from this point onwards.

The axial thermal noise profiles resulting from the vibration of a 5×5 central fuel assembly cluster in the three vibrational modes are shown in Fig. 8. As expected, higher neutron noise levels are obtained when larger number of fuel assemblies are vibrating simultaneously, as is the case with cluster vibrations. Note that all the fuel assemblies within the cluster are vibrating synchronously, i.e. with the same displacement amplitude and vibrational pattern. The highest noise levels are found to be 2.54%, 2.24%, and 2.03% for the cantilevered, C-shaped and S-shaped modes, which are, of course, higher than the ones obtained when a single fuel assembly is vibrating. The qualitative impact on the induced neutron noise profiles is consistent with the imposed vibrational modes.

In order to evaluate the effect on induced neutron noise due to the increasing distance of detectors from the noise source, a comparison of the axial noise distribution at the boundary of the vibrating cluster and along the neighboring fuel assemblies is shown in Fig. 9, where a central 5×5 cluster of fuel assemblies is vibrated sinusoidally in the three vibrational modes, along the x-direction. For all the vibrational modes, the induced neutron noise levels are higher in the adjacent fuel assembly, i.e. 1st neighbor of the vibrating cluster, Fig. 9 (top-right) compared to the fuel assembly located in the boundary of the vibrating cluster, Fig. 9 (top-left). Subsequently, the neutron noise levels continue to decrease for the 3rd neighbors, Fig. 9 (bottom-left) and for the peripheral fuel assembly located at the core-boundary, Fig. 9 (bottom-right). In case of the cantilevered mode vibration, the noise level near the core-top peaks at 2.5% in the 1st neighbor reduces to 1.17% already in the 3rd neighbor, and further decreases to 0.95% at the core-boundary. Therefore, the induced noise is the highest in the immediate vicinity of the noise source. Moreover, despite the change in the noise levels few mean free paths away from the noise source, the trend of the noise profile is preserved throughout. It is also seen that the induced neutron noise profile is skewed at the top. The tilt in the noise profile near the core-top is expected in case of cantilevered mode vibration due to the nature of such noise source as it introduces larger water-gap widths at the core-top compared to the core-bottom, however, the skewed behavior is also visible for both C- and S-shaped modes. This behavior is attributed to the decreased coolant density in the top region of the core, corresponding to a more negative moderator temperature coefficient.

It is worth noting that the axial noise distribution trends are unique to the core conditions of the reactor, and therefore, dependent on factors such as boron concentration and burn-up. In the Swiss pre-KONVOI PWR, it was found that at the beginning-of-cycle, the noise levels were higher at the core-top, whereas at the end-of-cycle, they were found to be higher at the core-bottom (Durrant et al., 2019).

The effect of the direction of vibration of the fuel assemblies can be derived from Fig. 10, where the radial neutron noise distribution at the core-mid plane is shown for the case of C-shaped mode vibration when the central fuel assembly (H8) and the central 5×5 fuel assembly cluster is vibrating in both x- and x-y-

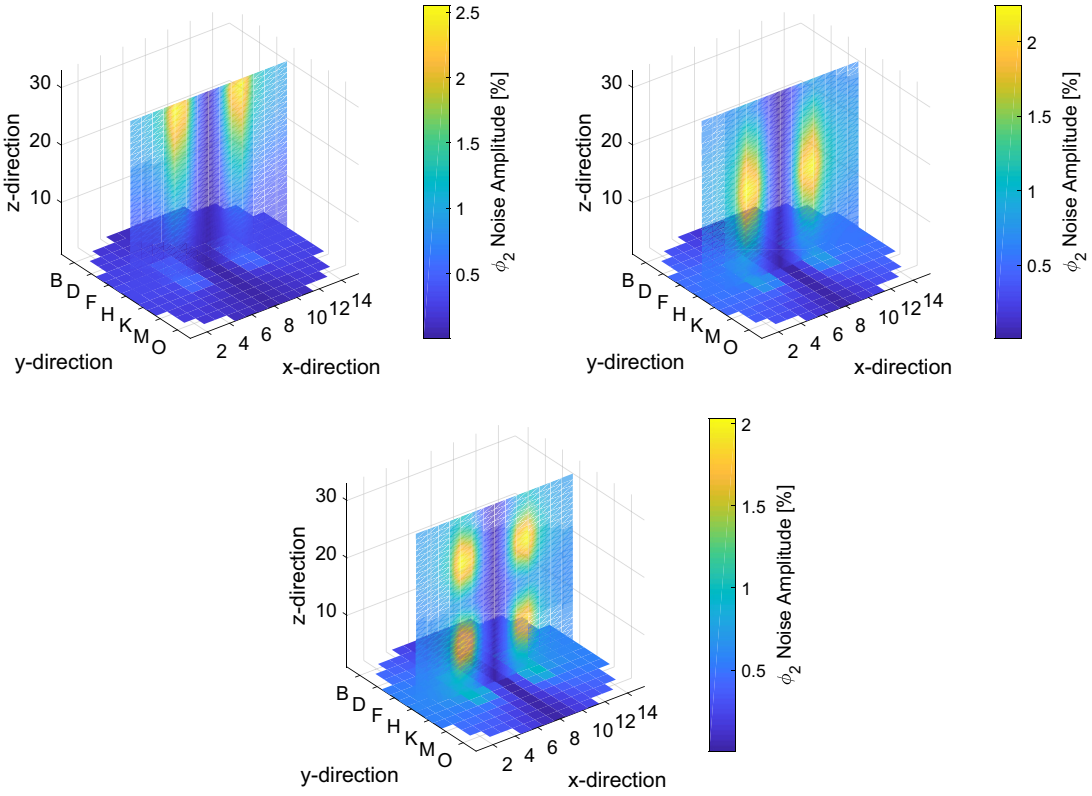

Fig. 8. Axial distributions of the induced neutron noise in thermal group due to 1 mm vibrations of a 5×5 central fuel assembly cluster in x-direction in the cantilevered mode (top-left), C-shaped mode (top-right) and S-shaped mode (bottom).

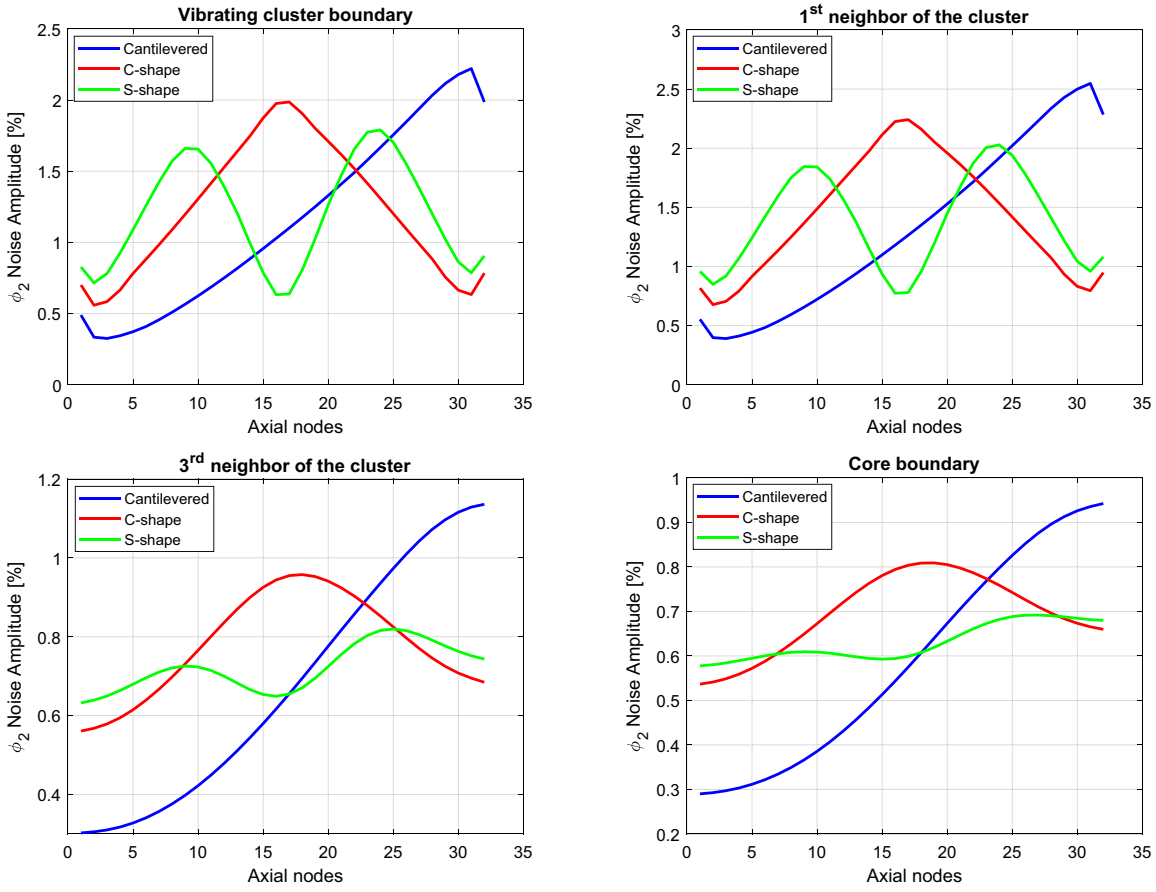

Fig. 9. Axial noise profile induced by a 5 × 5 fuel assembly cluster oscillation in the three vibrational modes along the x-direction at the boundary of the vibrating cluster (top-left), the 1st neighbor (top-right) and the 3rd neighbor (bottom-left) of the cluster, and the boundary of the core (bottom-right).

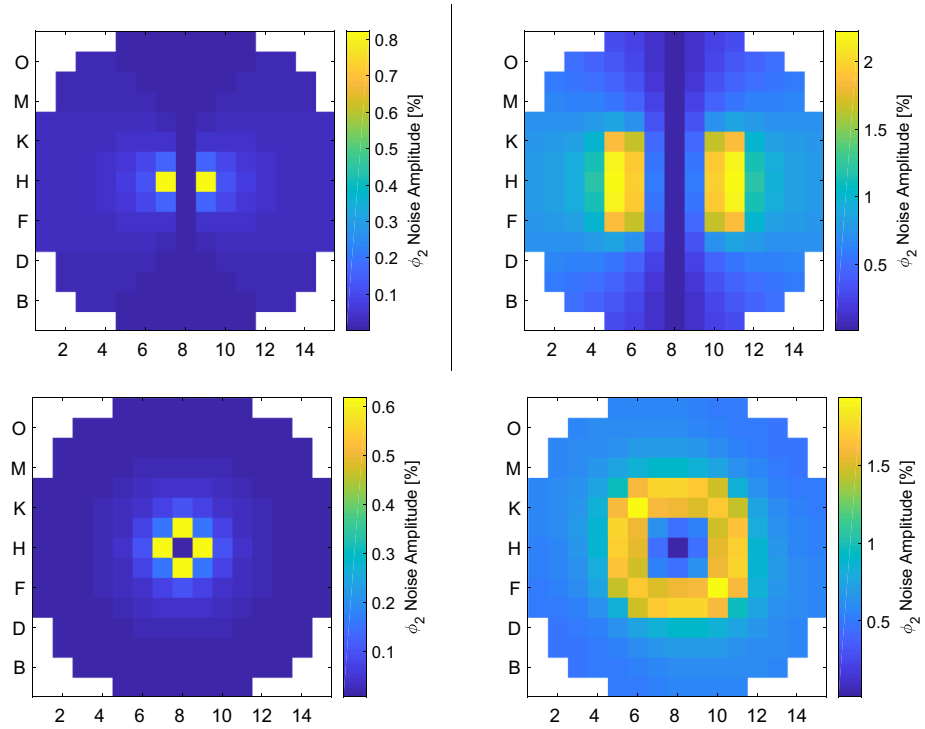

Fig. 10. Radial noise distribution at the core-middle due to C-shaped mode vibration of a central fuel assembly (left) and a 5 × 5 central fuel assembly cluster (right) in x-direction (top) and xy-direction (bottom) at 1.2 Hz and a displacement amplitude of 1 mm.

directions. In Section 3, it is discussed that the perturbed cross sections corresponding to the vibrating fuel assemblies' noise source are introduced in the eight sub-nodes belonging to the central and neighboring fuel assemblies, which results in cancellation of the cross sections in the four sub-nodes belonging to the central fuel assembly when the fuel assembly is vibrating. It shows that the relative movement of the central fuel assembly is zero compared to the rest of the moving cluster and the highest impact is seen on the first neighbors and the peripheral fuel assemblies of the vibrating cluster in the direction of motion. In Fig. 10 (top), the central fuel assembly and the 5 × 5 central fuel assembly cluster laterally vibrate along the x-direction, respectively, introducing the highest neutron noise in the adjacent fuel assemblies on either side. High neutron noise is also found at the periphery of the cluster itself. The behavior is slightly modified when the fuel assembly cluster vibrates along the combined x- and y-direction, as the maximum effect of such noise source is observed in the four adjacent fuel assemblies along the direction of motion. This is the case when the fuel assemblies are vibrating in a pure-sinuoidal manner. However, if the vibrations were introduced randomly, the induced noise is uniformly distributed azimuthally in all the directions, as seen in Fig. 10 (bottom), for both the central fuel assembly and the 5 × 5 central fuel assembly cluster, respectively.

In addition to the evaluation of the profiles of the neutron noise amplitudes, another useful quantity to study is the phase of the induced neutron noise across the core. An out-of-phase behavior is expected between the two halves of a symmetric reactor core when a central fuel assembly is vibrated. The axial node, where the induced neutron noise is the highest, is used for the evaluation. The out-of-phase response is seen in Fig. 11, where the central fuel assembly cluster is vibrated sinusoidally at 1.2 Hz in the cantilevered mode, C-shaped and S-shaped modes, respectively. The phase change is slightly non-symmetric around the center of the core at the 8th node because of the coarse nodal mesh size. The phase response supports the validity of the implemented methodology for fuel assembly vibrations.

4.2. Core barrel vibrations

As mentioned in Section 3, a core barrel vibration in beam mode can be visualized to be equivalent to a collective vibration of all the fuel assemblies in the core. As the core barrel is vertically suspended from the core-top, the noise source is modelled as simultaneous vibrations of fuel assemblies clamped from the top and moving freely at the bottom, as in the cantilevered vibrational mode. The radial and axial induced thermal neutron noise distribution due to vibration of core barrel in the x-direction is shown in Fig. 12 (top). Since, in reality, noise information must be obtained from the very few neutron detector signals available in the core, the noise levels simulated by the in-core and ex-core neutron detectors are also shown in Fig. 12 (bottom-left).

When all the fuel assemblies are vibrating simultaneously in a synchronous manner, only the peripheral layer of fuel assemblies and the surrounding radial reflector witness a net change in the water-gap widths around the core. The water-gap widths surrounding the rest of the fuel assemblies are unaltered as their relative motion is zero compared to the peripheral fuel assemblies. This effect is visible in Fig. 12 (top-left), where the neutron noise is seen to be symmetrically distributed along the outer edge of the core at the bottom axial level. Here, the radial noise distribution is shown at the axial level where it is the highest. As the neutron noise source is modelled in way such that the core barrel is clamped at the top, larger water-gap width is introduced at the bottom of the core compared to the top. The axially skewed neutron noise profile in Fig. 12 (top-right) and the monotonic decrease in the overall noise levels in the in-core and ex-core neutron detectors from the bottom of the core to the top, as seen in Fig. 12 (bottom-left) confirms the model. Also, amongst the noise response in the in-core neutron detectors in Fig. 12 (bottom-left), azimuthal detectors J2 and G14 consistently see the highest noise response axially along the core due to their proximity to the core-boundary in the direction of motion (refer to Fig. 3). The remaining azimuthal in-core neutron detectors see a symmetric decrease in the noise levels as the distance of the sensors from the noise source increases. Additionally, results from the neutron noise spectral analysis are shown in Fig. 12 (bottom-right). The power spectral density plot presents a peak at 8 Hz that corresponds to the beam mode vibration of core barrel.

It is also observed that the phase difference between the signals from the ex-core neutron detectors at the core-bottom, 'Lev 1', located opposite to each other is 180° at the desired frequency 8.0 Hz, as shown in Fig. 13 (left). The plots are shown for a reference ex-core neutron detector, S1. The core appears to be split in half in the direction of core-barrel motion, i.e. x-direction. Signals from detector pairs S1-S3 and S1-S4 are out-of-phase with each other. Signal from detector pair from the same side of the core-half, i.e. S1-S2 are in-phase with each other.

4.3. Thermal-hydraulic fluctuations

The neutron noise distributions due to time-dependent stochastic fluctuations of inlet coolant temperature and inlet coolant flow are shown in Figs. 14 and 15, respectively.

In Fig. 14, the plots show the radial and axial distribution of thermal neutron noise when the inlet coolant temperature fluctuates synchronously in all the four loops by 1 °C (~1.8 °F). The radial distribution is shown at the core-bottom level. The neutron noise is distributed uniformly radially across the core. Higher noise is

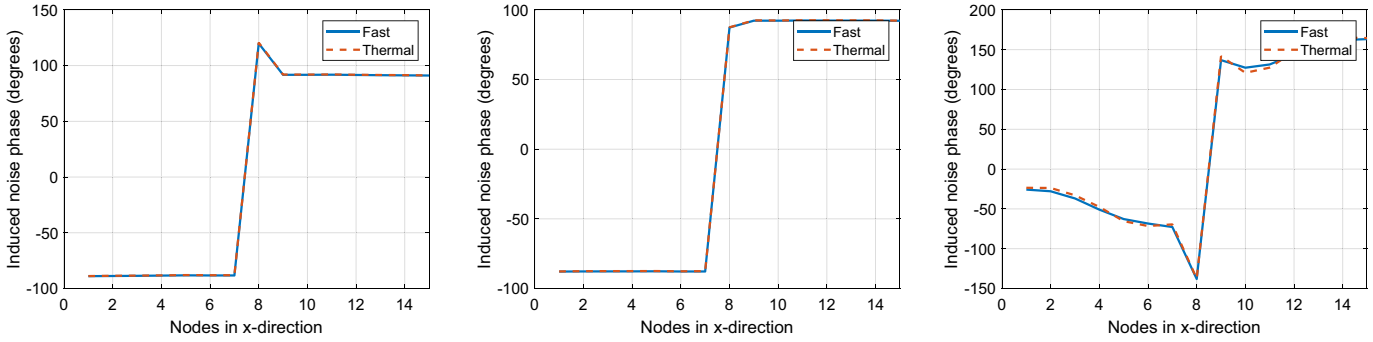

Fig. 11. Induced neutron noise phase distribution along the nodes in the x-direction due to vibration of a 5 × 5 cluster of fuel assemblies in cantilevered mode (left), C-shaped (middle) and S-shaped (right) mode.

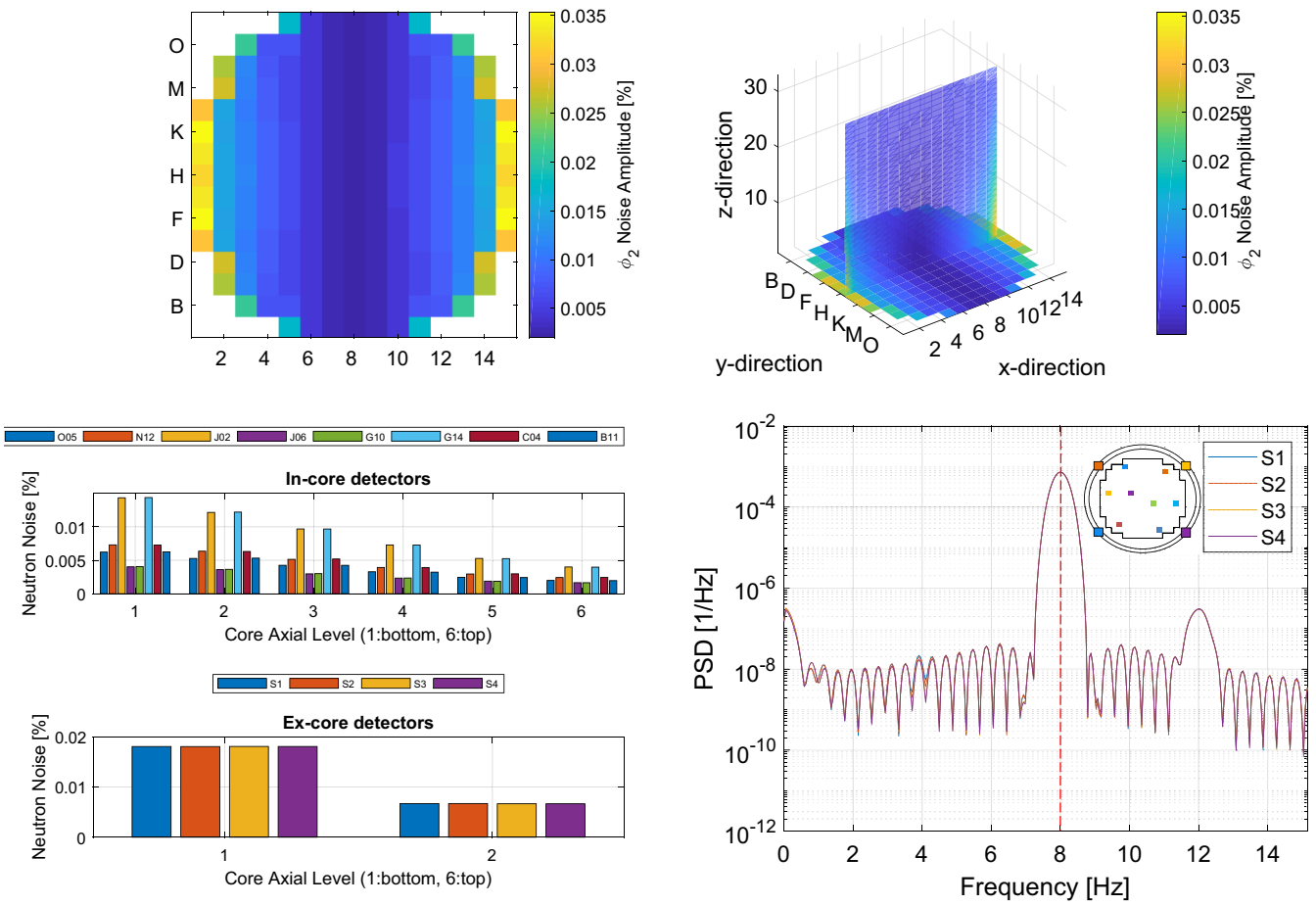

Fig. 12. Top: Radial (left) and axial (right) neutron noise distribution due to core barrel vibrations of 0.06 mm in beam-mode at 8 Hz; Bottom: Noise response (left) in in-core and ex-core neutron detectors, and the power spectral densities (right) obtained with the four ex-core neutron detectors, S1, S2, S3 and S4 at core-bottom. The dashed red line represents the vibration frequency of the core barrel.axial func.

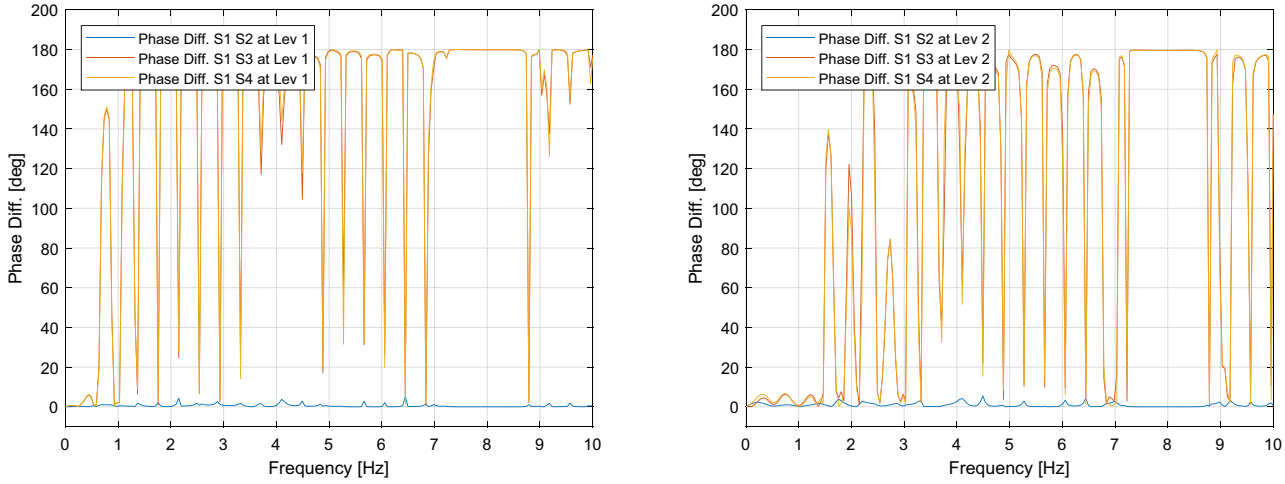

Fig. 13. Phase difference between ex-core neutron detectors, S1 ,S2, S3 and S4 at two axial levels, Lev 1 (left) and Lev 2 (right), with S1 as a reference. *Lev 1* corresponds to core-bottom and *Lev 2* corresponds to core-top.

observed at the bottom of the core, closer to the coolant loops. The propagation of the effect of inlet coolant temperature fluctuation is slow and delayed as it travels upwards with decreasing impact. Similarly, in Fig. 15, the radial and axial noise distributions are obtained by fluctuating the coolant flow in all the four loops of the reactor. The radial distribution is shown at the core-top level. In this scenario, the coolant flow propagation across the core is instantaneous with a negligible delay; the induced noise is almost

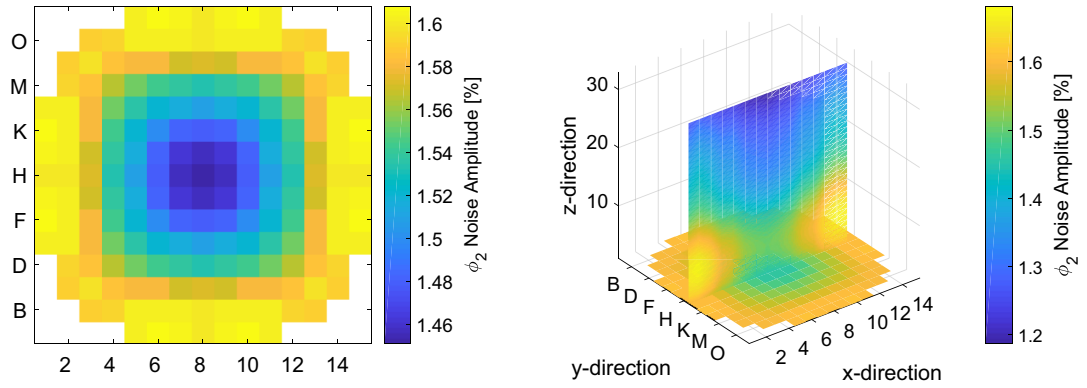

Fig. 14. Radial and axial thermal neutron noise distributions due to inlet coolant temperature in case of 1 °C fluctuation in all the four loops.

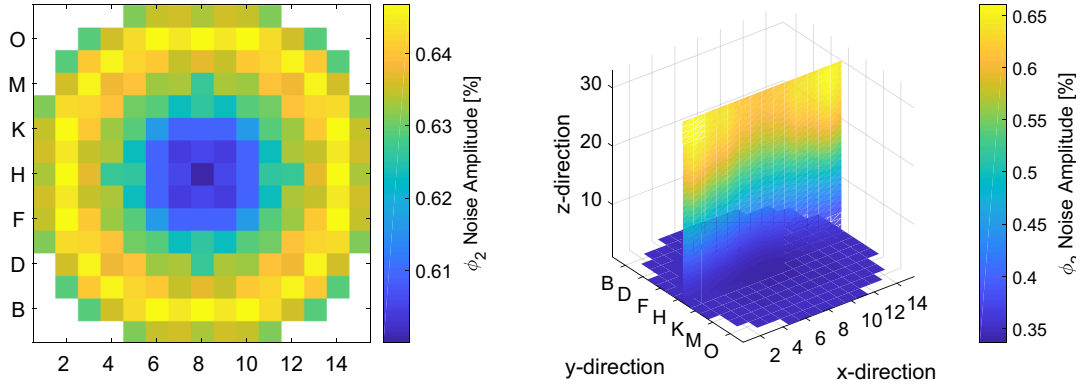

Fig. 15. Radial and axial thermal neutron noise distributions due to inlet coolant flow in case of 1% fluctuation in all the four loops.

the same at all axial levels. However, due to the low coolant density at the core-top, the highest neutron noise levels are obtained at the core-top axial level.

The instantaneous nature of the propagation of inlet coolant flow fluctuation to the top of the core is due to the coolant compressibility properties, while the propagation of inlet coolant temperature fluctuations is dependent on the operating transport phenomena along the thermal–hydraulic channels. It is also seen that the effect of inlet temperature fluctuations is larger than that of the inlet flow fluctuations in terms of the induced neutron noise amplitudes and the associated noise spectra in the lower frequency ranges of <2 Hz, as seen in Fig. 16.

4.4. Combination of noise scenarios

Two combinations of noise sources due to fuel assembly vibrations and thermal–hydraulic fluctuations are modeled in this section. First, in order to gauge the impact of the individual noise

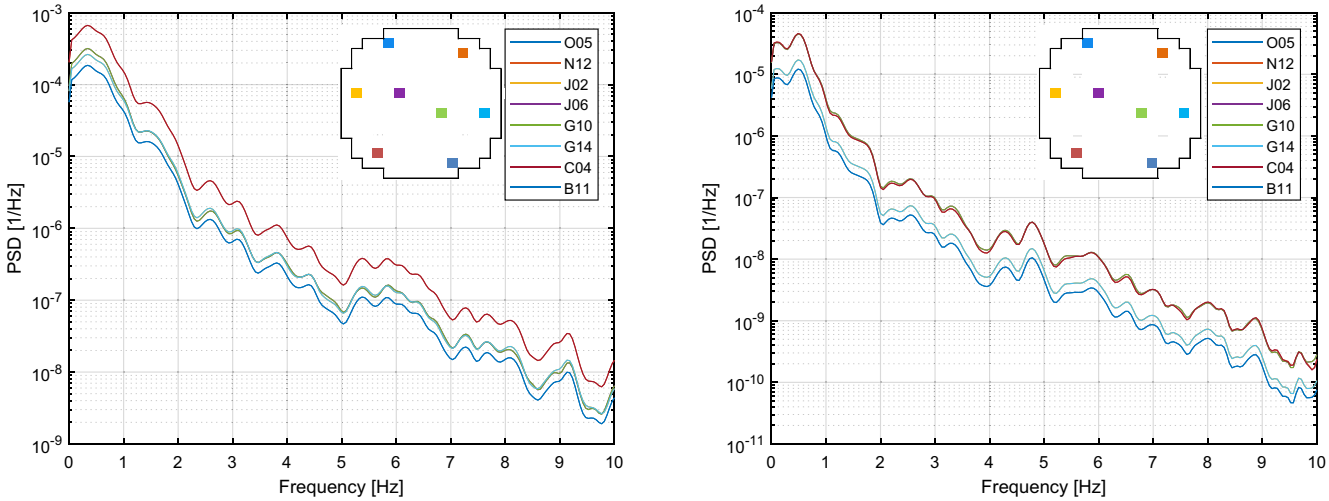

Fig. 16. Power spectral densities of azimuthal detector signals in case of fluctuations in inlet coolant temperature at core-top (left) and inlet coolant flow at core-bottom (right).

sources, a cantilevered mode vibration of fuel assemblies is simulated alongside synchronous fluctuations in inlet coolant temperature and coolant flow. Then, a realistic combination scenario with multiple cluster vibrations along with the thermal–hydraulic fluctuations is modeled. A summary of the fluctuation parameters for the two combination scenarios is given in Table 2.

4.4.1. Combination scenario-I

In this scenario, a superposition of a cantilevered mode fuel assembly cluster vibration with synchronous thermal–hydraulic fluctuations is modeled and their impact on the noise profiles is assessed. The scenario, as described in Table 2, includes vibration of a 5 × 5 central cluster of fuel assemblies with a maximum displacement of 0.1 cm in the x-direction at 1.2 Hz and synchronous fluctuations in inlet coolant temperature and inlet coolant flow by 1 °C and 1% relative value, respectively. The radial and axial noise profiles are shown in Fig. 17. The symmetric response of vibration of a fuel assembly cluster in cantilevered mode, as seen previously in Fig. 8, is visible in this scenario as well, even though synchronous thermal–hydraulic perturbations have been introduced. The effect of vibration of the 5 × 5 central cluster of fuel assemblies dominate over thermal–hydraulic fluctuations at the core-top, and therefore, the noise levels are higher at the core-top, as expected in case of a separate cantilevered mode fuel assembly vibration.

In order to evaluate the influence of individual noise sources in the Combination scenario-I, neutron noise levels seen by the in-core neutron detectors in case of a vibration of a 5 × 5 central cluster of fuel assemblies, inlet temperature fluctuation, inlet-flow fluctuation and their combination, respectively, are shown in Fig. 18. In case of individual thermal–hydraulic fluctuations, the in-core neutron detectors closest to the four coolant loops, i.e. O05, N12, J02, G14, C04, and B11, exhibit the highest noise levels as seen in Fig. 18 (top), whereas in case of vibration of central cluster, it is the central-most detectors i.e. J06 and G10 that observe the highest noise levels, as seen in Fig. 18 (bottom-left). Noise levels are found to increase with the axial level of the in-core neutron detectors in case of inlet coolant flow fluctuations and vibration of central cluster of fuel assemblies, whereas the noise levels tend to decrease axially in case of inlet coolant temperature fluctuations. This behavior is consistent with what has been shown previously in Section 4.1 and 4.3. When the noise sources are superimposed, the in-core neutron detectors closer to the coolant loops have higher noise levels, as seen in Fig. 18 (bottom-right). As we move axially to the top, the central detectors next to the vibrating cluster i.e. J06 and G10 show higher noise levels.

It is also observed that the sum of the noise levels obtained due to individual perturbations is not always equal to the noise levels obtained due to their superposition, as in the combination scenario-I. For instance, in Fig. 18 for detector J06, the noise level of ~2.2% at core axial level '6′, i.e. core-top for the combination scenario is lower than the sum of individual contributions, which is ~3.5%. There is an evidence of non-linearity in the noise response obtained with the time-domain based commercial nodal code S3K. There are possibly some higher-order effects that contribute to the non-linear noise response. Most of the dedicated noise solvers, however, are unable to capture such effects as they are based on linear noise theory.

Fig. 19 shows the power spectral densities of in-core neutron detector signals at the core-top in case of inlet coolant temperature fluctuation, inlet coolant flow fluctuation, vibration of a 5 × 5 central cluster of fuel assemblies, and their combination as simulated in Combination scenario-I. The effect of thermal–hydraulic fluctuations are seen in the lower frequency ranges of <2 Hz (Fig. 19 (top)), and the signature frequency due to vibration of central cluster of fuel assemblies is observed at 1.2 Hz in Fig. 19 (bottom-left). When the noise sources are combined, the signature frequencies of individual noise sources are still visible on the power spectral density plot, as seen in Fig. 19 (bottom-right), albeit the resonance peak corresponding to the cluster vibration is shifted towards the lower side of the spectrum.

The shift in the resonance frequency of the vibrating fuel assembly is found only in cases where fuel assemblies vibrations are modeled in combination with thermal–hydraulic fluctuations. In this approach, the power spectral density of a signal is obtained with the standard fourier transform method, where the APSD is defined as the Fourier transformation of the signals' autocorrelation function. In another approach that is not included here, the power spectral density can be obtained using the Autoregressive functions (AR), that are based on coefficients obtained by using Yule-walker equations on the discrete-time signals and then performing Z transform. In both the approaches, the frequency shift is consistently visible on the noise spectrum. The frequency shift is also observed in related works that employ other codes and approaches (Viebach et al., 2019; Montalvo et al., 2016), however, the behavior is not yet identified and discussed. A detailed and advanced signal analysis is beyond the scope of this study.

4.4.2. Combination scenario-II

Following recent developments in the PSI noise analysis methodology, it is now possible to model and simulate combination of noise sources with varying vibrational characteristics in terms of displacement amplitude and frequency. This is an attempt to simulate realistic scenarios of superposed perturbations in a reactor, where multiple fuel assembly clusters vibrate simultaneously with different frequencies and amplitudes. Therefore, in 'Combination scenario-II', a superposition of a cantilevered mode vibration of two fuel assembly clusters and thermal–hydraulic fluctuations are modeled, and their impact on the noise profiles is assessed. The scenario, as described in Table 2, includes vibration of a 5 × 5 central cluster of fuel assemblies with a maximum displacement of 0.1 cm in the x-direction at 1.2 Hz and a 3 × 3 cluster of fuel assemblies at the north-central core location with a maximum amplitude of 0.04 cm in the x-direction at 2.0 Hz, and synchronous fluctuations in inlet coolant temperature and inlet coolant flow by 1 °C and 1% relative value, respectively. Two different displacement amplitudes of fuel assemblies were chosen in order to observe comparable yet distinguishable noise distribution in the center and at the boundary of the core. The radial and axial noise profiles are shown in Fig. 20 (top). A visible change in the noise distribution is seen in two distinct regions in the core, one around the center of the core and another at the top core-

Table 2
Conditions of the simulated combination scenarios.

Scenarios	Cantilevered mode fuel assembly vibration				Thermal-hydraulic fluctuations	
	Cluster	Mode	Vibration frequency	Displacement amplitude	Inlet coolant temperature	Inlet coolant flow
Combination Scenario – I	5 × 5 central	Cantilevered	1.2 Hz	1.0 mm	±1 °C	±1%
Combination Scenario – II	5 × 5 central	Cantilevered	1.2 Hz	1.0 mm	±1 °C	±1%
	3 × 3 peripheral	Cantilevered	2.0 Hz	0.4 mm		

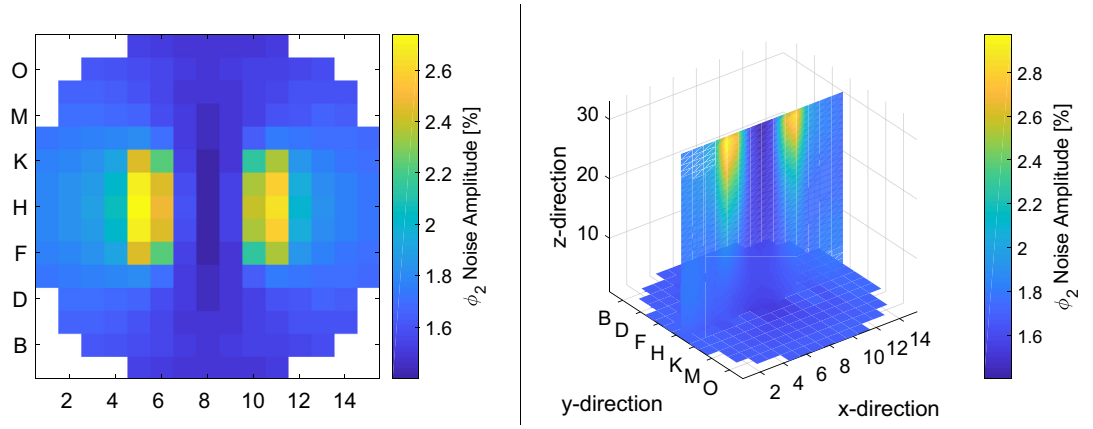

Fig. 17. Radial (core-top) and axial induced thermal noise distribution due to a superimposed noise sources, as described in Combination scenario-I.

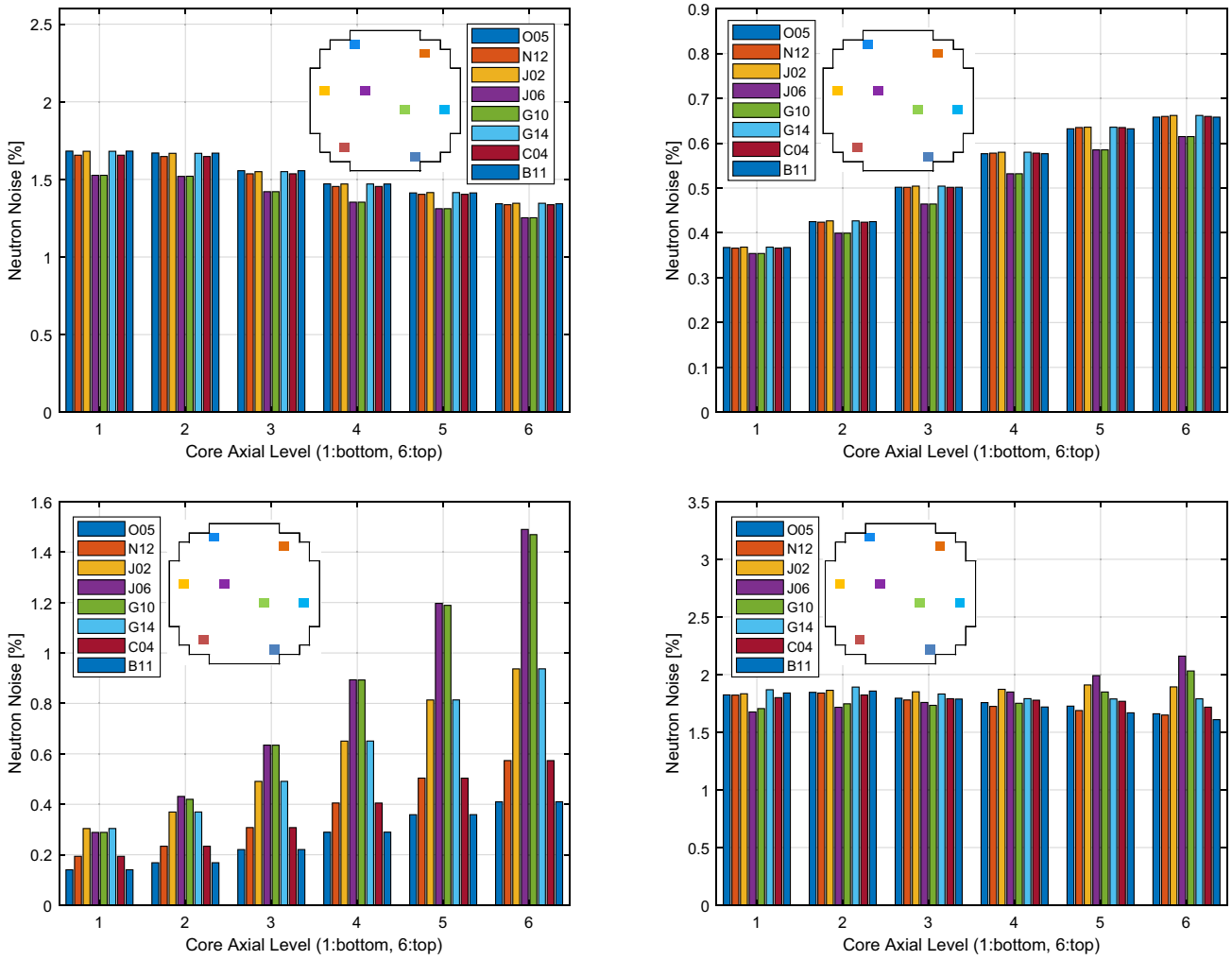

Fig. 18. Noise levels in in-core neutron detectors in the case of inlet temperature fluctuation (top-left), inlet-flow fluctuation (top-right), vibration of a 5 × 5 central cluster of fuel assemblies (bottom-left) and their combination, as described in Combination scenario-I (bottom-right).

boundary in Fig. 20 (top-left). The noise response of the vibration of central 5 × 5 fuel assembly cluster is symmetric around the center, while the response of the vibration of the 3 × 3 cluster close to the upper core-boundary is dominant towards the left half of the core. The latter's behavior is due to the proximity of the vibrating cluster to the core-boundary and reflector that introduces asymmetricity in the noise distribution. The environment surrounding the peripheral cluster is non-symmetric, which leads to the skewed noise distribution. A preliminary discussion is introduced regarding the effect of location of vibrating fuel assembly on the induced neutron noise amplitude and phase in Section 5, details of which is beyond the scope of this paper. The uniform distribution of neu-

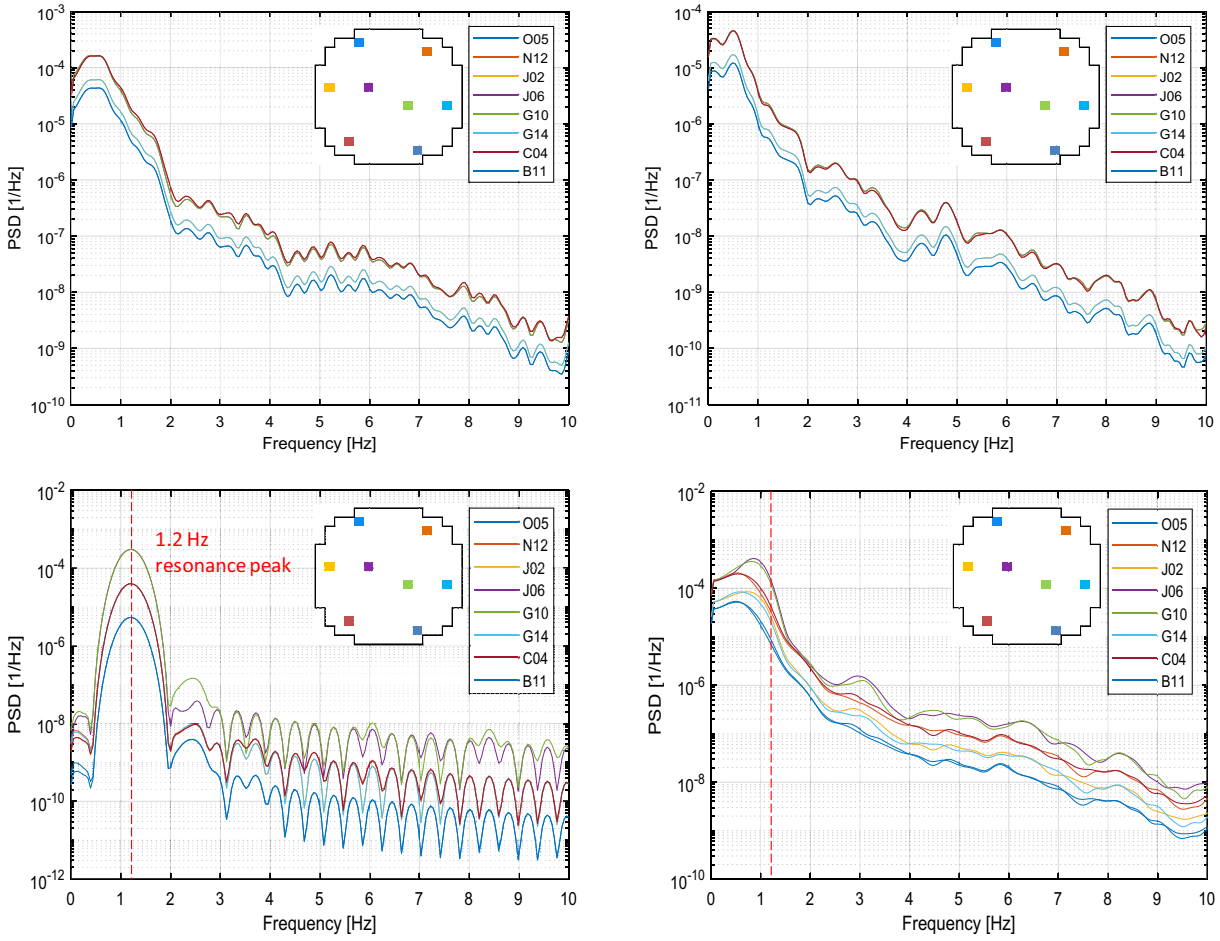

Fig. 19. Power spectral densities of in-core neutron detector signals at the core-top in case of inlet temperature fluctuation (top-left), inlet-flow fluctuation (top-right), vibration of a 5 × 5 central cluster of fuel assemblies (bottom-left) and their combination, as described in Combination scenario-I (bottom-right). The dashed red line represents the vibration frequency of the fuel assemblies.

tron noise at the core-bottom and core-top due to fluctuations in inlet coolant temperature and coolant flow separately, are not dominant in the noise profile of the superposed scenario.

Noise level distribution in the eight azimuthally located in-core neutron detectors at all axial levels are shown in Fig. 20 (bottom-left). The dominance of the effect of the thermal–hydraulic perturbations, especially inlet coolant temperature, in the detectors located close to the four coolant loops is seen only at the lower axial levels, till core axial level '3'. The overall increase in the noise levels in detectors 'O05', 'J06' and 'G10' from core-bottom to core-top is a result of the cantilevered-mode vibration of the two clusters of fuel assemblies, which is the overall dominant noise source in the combination of perturbations simulated here. This is expected because the detector 'O05' is located close to the vibrating 3 × 3 cluster near the upper core-boundary, while the detectors 'J06' and 'G10' are located next to the vibrating central 5 × 5 cluster of fuel assemblies. The frequency signatures corresponding to the introduced noise sources are seen in the power spectral densities distribution in Fig. 20 (bottom-right). Within this superposed scenario, it is still possible to identify two peaks corresponding to the 3 × 3 cluster and 5 × 5 cluster vibration, albeit they are shifted towards lower end of the spectrum. As several noise sources coexist in a reactor core, the flexible modelling approach of the current model allows to simulate superposed realistic scenarios that are possible in a PWR, and provide an understanding of their impact on the induced neutron noise in the core.

5. Effect of location of vibrating fuel assembly

The presence of an out-of-phase response between harmonic signals is used to localize the source of oscillation in a system, and consequently, is considered as one of the characteristic features for identification of fuel assembly vibrations. However, the phase response of the induced neutron noise due to a vibrating fuel assembly is found to be difficult to predict, as there are several factors that influence the behavior. In Fig. 11, it was already shown that an out-of-phase response is obtained between the two halves of a symmetric reactor core when a central fuel assembly is vibrated. Additionally, the phase difference between the noise responses at the neighbors of the vibrating fuel assemblies are evaluated here. Due to the limited in-core neutron detector locations available in the core, nodal thermal fluxes have been used to evaluate the phase functions between the closest neighbors for demonstrating phase response instead of the induced noise simulated by the detectors. Simulations have been performed for three fuel assemblies vibrating in cantilevered-mode, located in Region I (red), Region II (blue) and Region III (yellow), as marked in Fig. 21. The phase differences between two 1st neighbors and two 2nd neighbors on either side of the vibrating fuel assembly in terms of phase functions are shown in Fig. 22. During a fuel assembly vibration, the induced noise signals from the two neighboring fuel assemblies on either side of the vibrating fuel assembly should have a phase difference of 180°. It is seen that this behavior

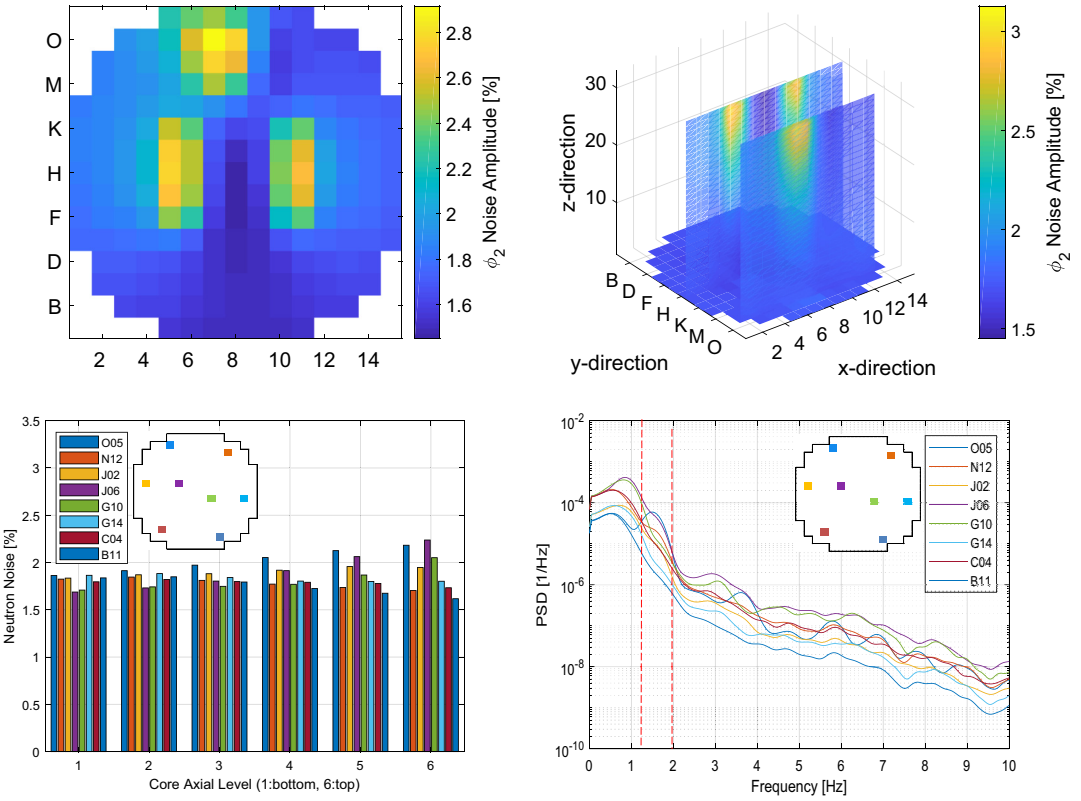

Fig. 20. Radial (core-top) and axial induced thermal noise distribution (top-left and top-right, respectively) due to a superimposed noise sources, noise level distribution (bottom-left) at azimuthal detector locations, and the power spectral densities (bottom-right) of the azimuthal detectors at the core-top in case of Combination Scenario-II. The dashed red line represents the vibration frequencies of the two clusters of fuel assemblies.

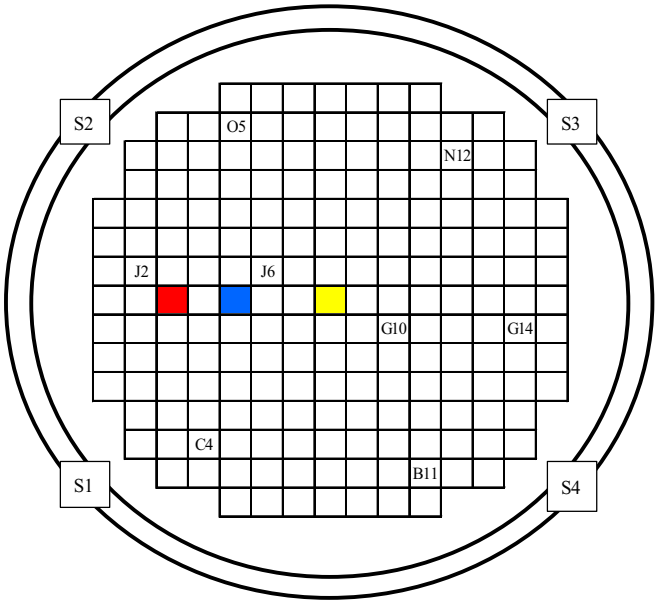

Fig. 21. Core layout with locations of vibrating fuel assemblies: Region I (red), Region II (blue) and Region III (yellow).

holds true for the cases where the fuel assembly is vibrated in Regions II and III. An out-of-phase response is seen at the desired frequency of 1.2 Hz between both the 1st and the 2nd neighbors on the opposite side of the vibrating fuel assembly. However, a departure from the out-of-phase behavior is observed in the phase response when a fuel assembly is vibrated near the boundary of the core, away from the center. In this case, the 2nd neighboring fuel assemblies vibrate almost in-phase at 1.2 Hz, which is the specific frequency at which the vibrating fuel assembly noise source is introduced. The 1st neighbors of the fuel assembly vibrating at Region I are out-of-phase, though.

The out-of-phase response of the induced neutron noise seems to be valid for symmetric systems only. This behavior can be further explained by evaluating the radial distribution of noise across the core for all the three cases, shown in Fig. 23. For a centrally vibrating fuel assembly as in Region III, the induced neutron noise is distributed symmetrically across the core, dividing the core in two equal halves. For an off-center vibrating fuel assembly as in Region II, the radial noise is distributed almost symmetrically in the first few neighbors, beyond which the noise is higher closer to the core-boundary. For the fuel assembly vibrating very close to the core-boundary as in Region I, the radial noise is highly asymmetric around the vibrating assembly. In the case of peripherally vibrating fuel assembly, there is a variation in the reactivity around the noise source, which results in a stronger point-kinetic component, with no phase change compared to the space-dependent component of the induced noise (Demazière, 2017). The discussion of the theoretical basis of the noise theory is out of the scope of this work. The aspects of phase response of the induced noise due to fuel assembly vibrations in a PWR discussed here need further investigations, and future work is planned in this direction.

6. Limitations of the model

The current PSI methodology for neutron noise modelling and analysis is able to model realistic fuel assemblies' vibrations with the possibility to model simultaneously vibrating fuel assemblies with different vibrational characteristics in terms of amplitude

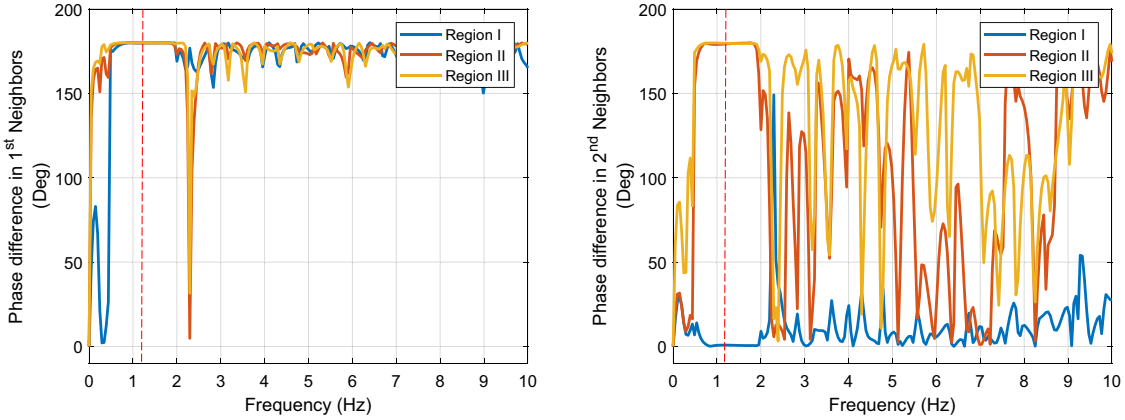

Fig. 22. Phase difference between 1st neighbors (left) and 2nd neighbors (right) due to vibration of a single fuel assembly in a pure-sinusoidal manner at 1.2 Hz with a displacement amplitude of 0.1 cm in Region I, Region II and Region III. The dashed red line represents the vibration frequency of the vibrating fuel assembly.

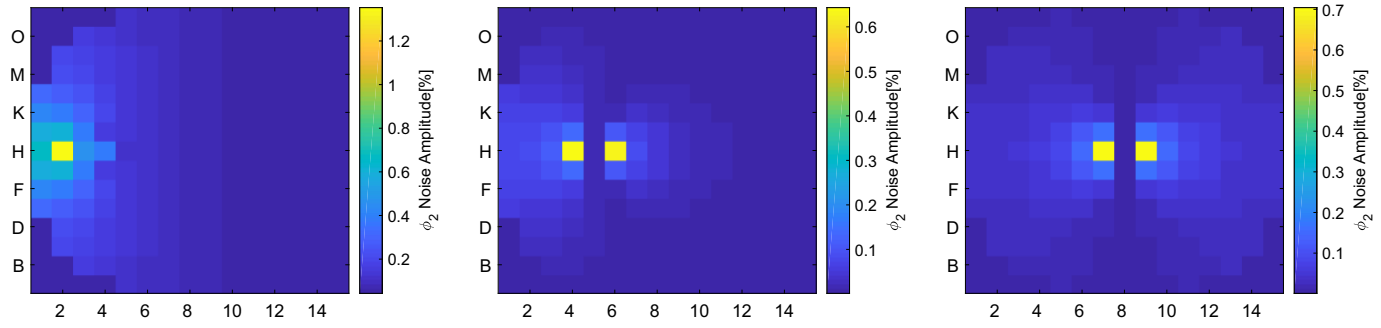

Fig. 23. Radial distribution (core-top) of induced thermal neutron noise due to vibration of a single fuel assembly in a pure-sinusoidal manner at 1.2 Hz with a displacement amplitude of 0.1 cm in Region I, Region II and Region III.

and frequency, and patterns such as random or sinusoidal movements. Despite such improvements, the assembly vibration model in the transient nodal code S3K has several limitations. The assembly vibration model is able to assign only one form of time-dependent axial shape to the chosen vibrating fuel assemblies. It is not possible to impose varied time-dependent axial shapes, representative of higher oscillation modes on multiple simultaneously vibrating fuel assemblies. In reality, the vibrational behavior of the fuel assemblies, which is defined by the vibrating frequency, amplitude and the oscillation mode is dependent on the conditions of the core, i.e. core loading and type of fuel assembly, and it is likely that several fuel assemblies simultaneously vibrate with different patterns in the core. Therefore, it would be worthwhile to include further flexibility in fuel assembly vibrations' modelling in the S3K code. In addition, the current S3K based fuel assembly modelling scheme uses external MATLAB scripts to prepare support files containing time-dependent delta-gap widths. As the external support files to be used with the S3K input are limited by size, it is not possible to perform long transients for full core vibrations with the current S3K version. This issue particularly concerns core barrel vibrations where all the fuel assemblies in the core are vibrated simultaneously. Therefore, it would be desirable to incorporate the in-house MATLAB-based scripts as subroutines in the S3K code and further simplify the noise analysis methodology.

7. Conclusions

This research work is an attempt to contribute towards the understanding of the increasing trend of neutron noise levels in KWU pre-KNVOI PWRs operating across Europe, where the primary suspects are believed to be the vibrations from core internals. The goal is to develop neutron noise analysis techniques for effective detection, identification and determination of location of such in-core perturbations responsible for the increased noise levels. To that aim, the current work presents an improved neutron noise methodology to model most plausible noise sources such as realistic vibrations of fuel assemblies in higher modes, and core barrel vibrations and their combination with the thermal-hydraulics fluctuations, and assess their impact on the induced neutron noise. A three-dimensional neutron noise distribution is obtained by performing signal processing of the time-dependent nodal neutron fluxes and the in-core and ex-core neutron detector signals simulated using the transient nodal code S3K. The noise analysis is based on the evaluation of the neutron noise levels and power spectral densities of the signals and studies of their characteristic responses.

Results show that the introduction of noise sources based on vibrations of fuel assemblies at higher vibrational modes and core barrel vibrations, and their combination with thermal–hydraulic perturbations have an identifiable effect on the neutron noise phenomenology. The radial and axial distributions of the induced neutron noise due to vibrations of fuel assemblies in cantilevered mode, C-shaped and S-shaped mode follow the time-dependent complex perturbations introduced as noise sources within the assembly vibration model in S3K. The radial noise profiles show that higher noise amplitude is obtained in regions where the displaced gap around the vibrating fuel assembly is larger, and the perturbation due to vibrating fuel assemblies induce highest impact in the assemblies adjacent to the vibrating cluster as the modification of water-gap widths impact the 1st neighbors and

the fuel assemblies at the boundary of the vibrating cluster the most. The axial noise profiles reveal that noise amplitude is higher near the core-top compared to the core bottom for all vibrational modes because of the decreased coolant density in the top region of the core, which corresponds to a more negative moderator temperature coefficient. Post-processing of the simulated neutron noise in the frequency domain shows that the vibrating frequencies of the fuel assemblies are observable in the noise spectrum. This behavior is found true for the core barrel vibrations as well, which further confirms the model.

The random fluctuations of inlet coolant temperature and flow introduced synchronously in the four coolant loops impact the noise spectrum in the low frequency range of <2 Hz. It is found that the inlet temperature fluctuation is the dominant noise source out of the two thermal–hydraulic perturbations, although, when multiple noise sources are introduced simultaneously, the impact of individual perturbations are still visible on the noise spectra. The two symmetric halves of the core demonstrate an out-of-phase behavior in case of core barrel vibration and centrally vibrating fuel assemblies. The lack of phase-shift observed in case of non-symmetric systems, i.e. peripheral perturbations, needs more investigation. Furthermore, the presence of non-linearity in the superposed noise response and the frequency shift observed in the power spectral densities obtained with the standard Fourier transforms for the noise scenario when fuel assembly vibrations are combined with thermal–hydraulic fluctuations, are yet unclear.

This study illustrates the maturity of the PSI neutron noise methodology to simulate realistic noise sources in real heterogeneous systems, and determine the induced neutron noise in the reactor core along with the noise spectra. Advantages of the transient nodal codes such as S3K include their ability to allow thermal–hydraulic feedback and inherently handle non-linear effects, and therefore, the possibility to capture higher-order effects of noise sources. In addition, the methodology is essential for the development of neutron noise monitoring system for the PWRs as it allows the user to generate simulated datasets for various different scenarios, representative of the real plant conditions as close as possible, as was done for the CORTEX consortium partners. The generated data is further used for advanced signal processing and training of machine learning algorithms for anomaly characterization and localization purposes by unfolding the detector signals, and later the techniques are applied on real plant data. The eventual goal is to use such techniques along with the simulation methods for both online and offline core diagnostics and monitoring of the PWRs.

As the methodology is based on the time-domain commercial lattice and nodal codes that are not intended primarily for modelling neutron noise sources, and were later adapted for noise analysis purposes, it is suggested to perform validation studies with the frequency-domain based code CORE SIM, which is dedicatedly used for neutron noise analysis applications. Furthermore, it is advisable to accommodate the limitations mentioned in the previous section in the future extensions of the methodology, and continue to investigate the open-ended aspects of the noise analysis introduced in this work.

CRediT authorship contribution statement

V. Verma: Conceptualization, Methodology, Formal analysis, Writing - original draft. **D. Chionis:** Conceptualization, Methodology, Writing - review & editing. **A. Dokhane:** Conceptualization, Methodology, Writing - review & editing, Funding acquisition. **H. Ferroukhi:** Writing - review & editing, Project administration.

Declaration of Competing Interest

The authors declare that they have no known competing financial interests or personal relationships that could have appeared to influence the work reported in this paper.

Acknowledgements

The current research has been carried out within the CORTEX research project, which has received funding from the Euratom research and training programme 2014–2018 under grant agreement number No. 754316.

References

Almaraz Trillo Report, 2012. Neutron noise status in Trillo NPP, technical report CO-12/043, Spain.
Bastl, W., Bauernfeind, V., 1975. The estimation of vibration of reactor internals by noise analysis of non-nuclear parameters. Ann. Nuc. 2 (2-5), 277–285.
Bermejo, J.A., Montalvo, C., Ortego, A., 2017. On the possible effects contributing to neutron noise variations in KWU-PWR reactor : modelling with S3K. Prog. Nucl. Energy. 95, 1–7.
Chionis, D., Dokhane, A., Belblidia, L., Ferroukhi, H., Girardin, G., Pautz, A., 2020. Development and verification of a methodology for neutron noise response to fuel assembly vibrations. Ann. Nucl. Energy 147,. https://doi.org/10.1016/j.anucene.2020.107669 107669.
Chionis, D., Dokhane, A., Belblidia, L., Pecchia, M., Girardin, G., Ferroukhi, H., Pautz, A., 2017. SIMULATE-3K analyses of neutron noise response to fuel assembly vibrations and thermal-hydraulics parameters fluctuations, in: Jeju, Korea.
Demazière, C., 2011. CORE SIM : a multi-purpose neutronic tool for research and education. Ann. Nucl. Energy 38, 2698–2718. https://doi.org/10.1016/j.anucene.2011.06.010.
Demazière, C., Dokhane, A., 2019. Description of scenarios for the simulated data, CORTEX D3.1.
Demazière, C., Dykin, V., Hernández-solís, A., Boman, V., 2015. Development of three-dimensional capabilities for modelling stationary fluctuations in nuclear reactor cores. Ann. Nucl. Energy 84, 19–30. https://doi.org/10.1016/j.anucene.2014.09.042.
Demaziere, C., Vinai, P., Hursin, M., Kollias, S., Herb, J., 2018. Overview of the CORTEX project, Proceedings of the International Conference on the Physics of Reactors – Reactor Physics paving the way towards more efficient systems (PHYSOR2018), Cancun, Mexico, April 22–26, 2018.
Demazière, C., 2017. Core Diagnostics Using Noise Analysis: From Proof-Of-Principle to Industrial Demonstration, Proceedings of the International Conference Mathematics & Computational Methods Applied to Nuclear Science & Engineering (M&C 2017), Jeju, Korea, April 16-20, 2017.
Durrant, A., Leontidis, G., Kollias, S., 2019. 3D convolutional and recurrent neutral networks for reactor perturbation unfolding and anomaly detection. EPJ Nuclear Sci. Technol. 5, 20. https://doi.org/10.1051/epjn/2019047.
Ferrer, R., 2015. CASMO-5 Methodology Manual (SSP-08/405 – Rev 4).
Gammicchia, A., Santandrea, S., Zmijarevic, I., Sanchez, R., Stankovski, Z., Dulla, S., Mosca, P., 2020. A MOC-based neutron kinetics model for noise analysis. Ann. Nucl. Energy 137,. https://doi.org/10.1016/j.anucene.2019.107070 107070.
Grandi, G., 2011. SIMULATE-3K Models & Methodology (SSP-98/13 Rev. 7).
Kozlowski, T., Downar, T.J., 2007. OECD/NEA and US NRC PWR MOX/UO2 core transient benchmark – Final Specifications – Revision 2, NEA/NSC/DOC (2006) 20, D.
Leppänen, J., Pusa, M., Viitanen, T., Valtavirta, V., Kaltiaisenaho, T., 2015. The Serpent Monte Carlo code: status, development and applications in 2013. Ann. Nucl. Energy. 82, 142–150. https://doi.org/10.1016/j.anucene.2014.08.024.
Montalvo, C., Pazsit, I., Nylen, H., 2016. First evidence of the pivotal motion (“tilting mode”) of the core barrel in the Ringhals-4 PWR. Physor, 2571–2579.
Mylonakis, A.G., Vinai, P., Demaziere, C., 2020. Numerical solution of two-energy-group neutron noise diffusion problems with fine spatial meshes. Ann. Nucl. Energy 140,. https://doi.org/10.1016/j.anucene.2019.107093 107093.
Olmo-Juan, N., Demazière, C., Barrachina, T., Miró, R., Verdú, G., 2019. PARCS vs CORE SIM neutron noise simulations. Progr. Nucl. Energy 115, 169–180.
Pazsit, N., Karlsson, I., Garis, J., 1998. SOME DEVELOPMENTS IN CORE-BARREL VIBRATION DIAGNOSTICS, 25, pp. 1079–1093.
Pazsit, Imre, Demaziere, C., 2010. Noise Techniques in Nuclear Systems, Handbook of Nuclear Engineering, Springer US.
Rouchon, A., Zoia, A., Sanchez, R., 2017. A new Monte Carlo method for neutron noise calculations in the frequency domain. Ann. Nucl. Energy 102, 465–475. https://doi.org/10.1016/j.anucene.2016.11.035.
Seidl, M., Kosowski, K., Schüler, U., Belblidia, L., 2015. Review of the historic neutron noise behaviour in German KWU built PWRs. Progr. Nucl. Energy 85, 668–675.
Sweeney, C., March-Leuba, F., Smith, J., 1985. Contribution of fuel vibration to ex-core neutron noise during the first and second fuel cycles of the Sequoyah-1 pressurized water reactor. Prog. Nucl. Energy 15, 283–290.

Tasakos, T., Ioannou, G., Verma, V., Alexandridis, G., Dokhane, A., Stafylopatis, A., 2021. Deep-learning based anomaly detectionin nuclear reactor cores, Extended abstract, International Conference Mathematics & Computational Methods Applied to Nuclear Science & Engineering (M&C 2019), Rayleigh, North Carolina, April 11-15, 2021.

Thie, J., 1981. Power Reactor Noise, American Nuclear Society.

Torres, L.A., Chionis, D., Montalvo, C., Dokhane, A., García-Berrocal, A., 2019. Neutron noise analysis of simulated mechanical and thermal-hydraulic perturbations in a PWR core. Ann. Nucl. Energy 126, 242–252. https://doi.org/10.1016/j.anucene.2018.11.032.

Vidal-Ferràndiz, A., Carreño, A., Ginestar, D., Demazière, C., Verdú, G., 2020. A time and frequency domain analysis of the effect of vibrating fuel assemblies on the neutron noise. Ann. Nucl. Energy 137,. https://doi.org/10.1016/j.anucene.2019.107076 107076.

Viebach, M., Lange, C., Kliem, S., Demaziere, C., Rohde, U., Hennig, D., Hurtado, A., 2019. A comparison between time domain and frequency domain calculations of stationary neutron fluctuations. In: Proceedings of the International Conference Mathematics & Computational Methods Applied to Nuclear Science & Engineering (M&C 2019), Portland, Oregon, August 25-29, 2019.

Viebach, M., Lange, C., Bernt, N., Seidl, M., Hennig, D., Hurtado, A., 2019. Simulation of lowfrequency PWR neutron flux fluctuations. Progr. Nucl. Energy 117. 103039.

Yamamoto, Toshihiro, 2018. Implementation of a frequency-domain neutron noise analysis method in a production-level continuous energy Monte Carlo code: verification and application in a BWR. Ann. Nucl. Energy 115, 494–501. https://doi.org/10.1016/j.anucene.2018.02.008.